nature structural & molecular biology

ARTICLES

https://doi.org/10.1038/s41594-019-0196-z

A folded conformation of MukBEF and cohesin

Frank Bürmann[1], Byung-Gil Lee[1], Thane Than[2], Ludwig Sinn[3], Francis J O'Reilly[3], Stanislau Yatskevich[4,6], Juri Rappsilber[3,5], Bin Hu[2], Kim Nasmyth[4] and Jan Löwe[1*]

Structural maintenance of chromosomes (SMC)–kleisin complexes organize chromosomal DNAs in all domains of life, with key roles in chromosome segregation, DNA repair and regulation of gene expression. They function through the entrapment and active translocation of DNA, but the underlying conformational changes are largely unclear. Using structural biology, mass spectrometry and cross-linking, we investigated the architecture of two evolutionarily distant SMC–kleisin complexes: MukBEF from *Escherichia coli*, and cohesin from *Saccharomyces cerevisiae*. We show that both contain a dynamic coiled-coil discontinuity, the elbow, near the middle of their arms that permits a folded conformation. Bending at the elbow brings into proximity the hinge dimerization domain and the head–kleisin module, situated at opposite ends of the arms. Our findings favour SMC activity models that include a large conformational change in the arms, such as a relative movement between DNA contact sites during DNA loading and translocation.

All organisms maintain enormous chromosomal DNA molecules whose contour lengths exceed cellular dimensions by orders of magnitude. Hence, both regulation of gene expression and accurate chromosome segregation require a high degree of spatial organization. SMC–kleisin complexes are ancient machines that help to organize chromosome superstructure in bacteria, archaea and eukaryotes[1]. They are essential for chromosome segregation in many bacteria[2,3], and indispensable for both mitosis and meiosis in eukaryotes[4–8].

At the core of SMC–kleisin complexes is a conserved tripartite protein ring composed of an SMC homo- or heterodimer, bridged by a kleisin subunit[9–12]. SMC proteins are elongated molecules containing an ABC-type ATPase head and a hinge dimerization domain at opposite ends of an approximately 50 nm long intramolecular and antiparallel coiled-coil arm[9,13–16]. The kleisin asymmetrically connects the two heads of an SMC dimer and contains binding sites for additional KITE or HAWK subunits[17,18].

A widely conserved and possibly fundamental aspect of SMC–kleisin activity is the ability to entrap chromosomal DNA within their ring structure[19–21]. DNA entrapment is the molecular basis for sister chromatid cohesion by the cohesin complex, and might also be used by cohesin, condensin and bacterial Smc–ScpAB to organize DNA into large loops. Loading of DNA into the complex is thought to involve transient opening of a ring interface in cohesin[22,23], and is likely to be mediated by the SMC arms in Smc–ScpAB[24].

The second possibly universal aspect of SMC–kleisin activity is their translocation along DNA. Cohesin and bacterial SMC–kleisin complexes associate with chromosomes in a manner that requires ATP binding and they redistribute or translocate from initial loading sites to adjacent regions dependent on ATP hydrolysis[25–28]. Translocation of bacterial Smc–ScpAB coincides with progressive linking of distant chromosomal loci in vivo, indicating that the complex might actively extrude DNA loops[28,29]. Recently, ATPase-dependent DNA translocation and loop extrusion reactions have been reconstituted for purified condensin in vitro[30,31]. These findings support the idea that SMC–kleisin complexes are motor proteins that use the ATPase activity of their SMC subunits to track along DNA, and some, by doing so, might actively organize chromosomes by building up loops[32–34].

To explore how the core activities of SMC–kleisin complexes might be implemented on a structural level, we have investigated the architecture of two representative complexes that are separated by a billion years of evolution: MukBEF from *E. coli* and cohesin from budding yeast. We find that both complexes contain a bendable coiled-coil discontinuity in their arms that allows them to interconvert between extended and folded conformations, in the latter bringing the hinge dimerization domain closer to the head–kleisin module. Our findings show that SMC proteins have the capacity for a large conformational transformation, and provide the basis for investigating long-distance domain movements during DNA loading and translocation reactions.

Results

A folded conformation of MukBEF and cohesin. MukBEF is a diverged SMC–kleisin complex that serves as an essential chromosome-organization machine in *E. coli*[11,27,35,36]. The complex comprises the SMC protein MukB, the kleisin MukF and the KITE protein MukE. We co-overexpressed the MukBEF subunits in *E. coli* and prepared the complex using a multi-step procedure that yielded purified material without extra residues on any of the subunits (Fig. 1a). The purified complex eluted as a single peak in size-exclusion chromatography (SEC) (Fig. 1b) and was analyzed by negative-stain electron microscopy (EM) immediately after elution from the column (Fig. 1c,d). Although subject to heterogeneity, most particles had a characteristic double cherry-like shape, composed of a two-lobed density (the MukB head–MukEF module) from which a stalk emerged (the MukB arms). Surprisingly, many particles possessed a stalk length of about 24 nm, roughly half of what is expected for an extended MukB arm consisting of canonical coiled-coil segments. As evident from partially extended particles, this conformation was caused by folding at a kink close to the center of the MukB arms. We refer to this kink as the 'elbow', as it connects the upper and lower parts of the arms (Fig. 1d). Fully extended particles were also observed but were less apparent. Using

[1]MRC Laboratory of Molecular Biology, Cambridge, UK. [2]Department of Molecular Biology and Biotechnology, University of Sheffield, Sheffield, UK. [3]Bioanalytics, Institute of Biotechnology, Technische Universität Berlin, Berlin, Germany. [4]Department of Biochemistry, University of Oxford, Oxford, UK. [5]Wellcome Centre for Cell Biology, University of Edinburgh, Edinburgh, UK. [6]Present address: MRC Laboratory of Molecular Biology, Cambridge, UK. *e-mail: jyl@mrc-lmb.cam.ac

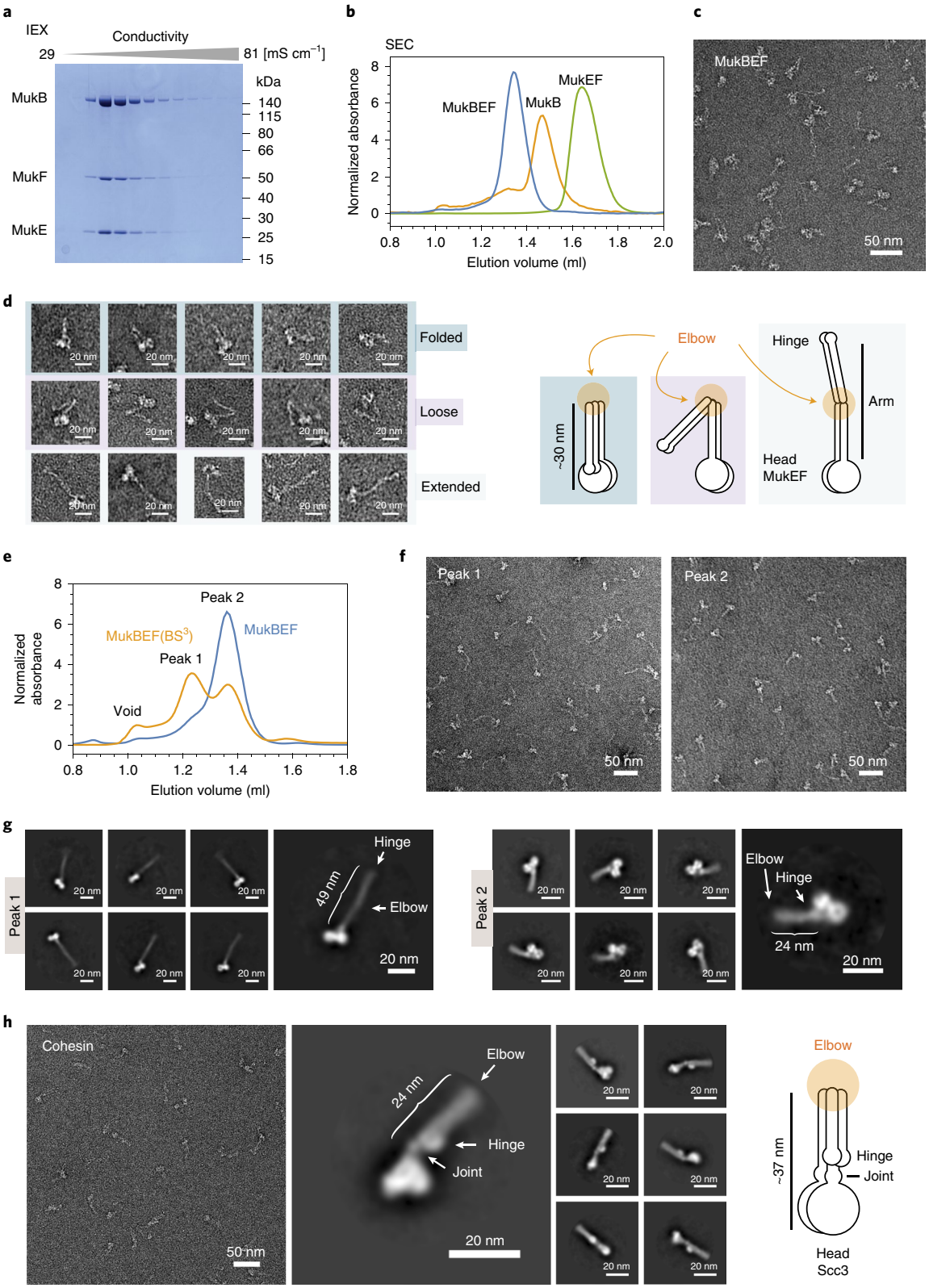

Fig. 1 | Folded conformation of MukBEF and cohesin. a, Purification of MukBEF. Elution of the MukBEF complex from a Q ion exchange (IEX) column. Peak fractions were separated by SDS-PAGE and stained with Coomassie blue. An uncropped gel image is shown in Supplementary Dataset 1. **b**, SEC of the MukBEF complex, MukB and MukEF. Proteins were separated on Superose 6 Increase. **c**, Negative-stain EM of native MukBEF. A typical field of view is shown. **d**, Particle instances for observed MukBEF conformations are shown on the left. A cartoon highlighting the position of the elbow is shown on the right. **e**, SEC profiles for native and MukBEF cross-linked with BS^3 are shown. **f**, Negative-stain EM of BS^3-cross-linked MukBEF. Typical fields of view for particles from SEC peak 1 and SEC peak 2 are shown. **g**, Negative-stain 2D class averages for extended (left) and folded (right) conformations, using circular masks of 948 Å and 640 Å, respectively. Data were collected from samples of peak 1 and peak 2 of the SEC shown in **e**. **h**, Negative-stain EM of BS^3-cross-linked cohesin. A typical field of view is shown on the left. Class averages using a circular mask of 500 Å are shown in the middle panel.

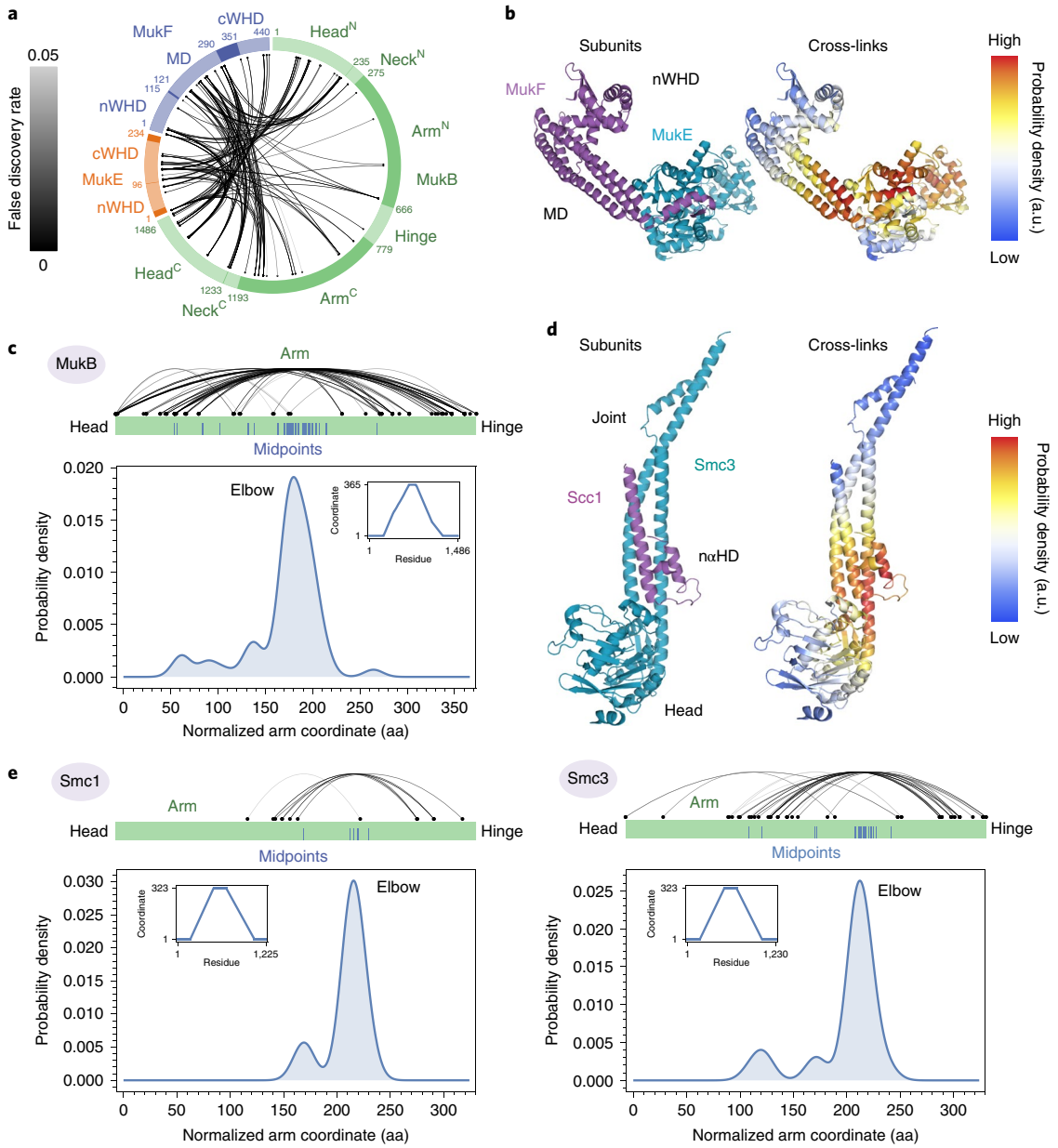

Fig. 2 | Elbow positions revealed by cross-linking and mass spectrometry. a, Inter-subunit cross-links of MukBEF. Links are colored according to their false discovery rate. **b**, Kernel density estimates for cross-link sites mapped onto the *E. coli* MukEF subcomplex (PDB ID 3EUH). **c**, Identification of the MukB elbow region. Cross-links greater than 100 aa apart in a coordinate system along the coiled-coil arm and their midpoints are shown on top. The bottom panel shows the kernel density estimate for the midpoint positions. An inset shows the piecewise interpolation function used to map residue numbers to the arm coordinate system. **d**, Kernel density estimates for cross-link sites mapped onto the cohesin Smc3–Scc1 interface (PDB ID 4UX3). **e**, Identification of the cohesin elbow region as in **c**. a.u., arbitrary units.

reference-free two-dimensional (2D) image classification, we obtained class averages for the conformationally less heterogeneous closed form (Supplementary Fig. 1a). Class averages displayed the MukB head–MukEF module as a bowtie shaped density with a central bridge and showed a clear signal for the folded arms with the elbow at its vertex. We also observed the presence of the elbow by cryo-EM imaging of a distantly related (~26% sequence identity) MukBEF complex embedded in vitreous ice, without the use of particle support or contrast agent (Supplementary Fig. 1b–d).

We noticed the presence of a considerable fraction of what appeared to be broken particles on the negative-stain EM grids, possibly caused by the grid-preparation procedure. To decrease heterogeneity, we subjected *E. coli* MukBEF to mild cross-linking with the amine-reactive compound BS^3 (bis(sulfosuccinimidyl)suberate). This treatment caused the complex to elute from SEC in two major peaks: one at a retention volume similar to native material, and one eluting earlier, indicative of an increased hydrodynamic radius (Fig. 1e). Electron micrographs of material eluting at a retention volume similar to that of native material revealed particles mostly in the folded conformation, with considerably reduced heterogeneity (Fig. 1f). The faster eluting fraction migrated differently from reconstituted MukBEF doublets[37] (Supplementary Fig. 2a) and was, interestingly, enriched for singlet particles in an extended conformation (Fig. 1f). We readily obtained 2D class averages for both open and closed conformations of BS^3-cross-linked MukBEF using this fractionation approach (Fig. 1g). In the averages, the MukB elbow is positioned

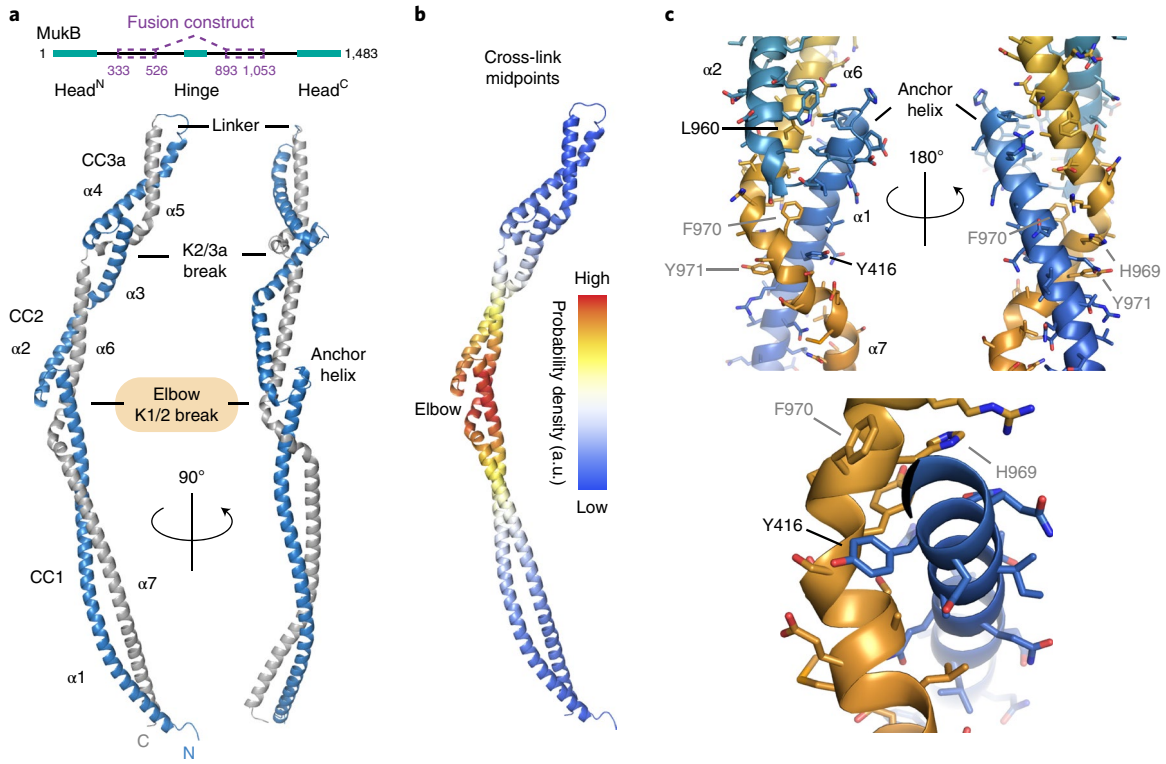

Fig. 3 | Structure of the MukB elbow. a, Crystal structure of an *E. coli* MukB arm fragment. The top panel illustrates the design of the fusion construct used for crystallography. The bottom panel shows the refined atomic model obtained from the X-ray diffraction experiment. **b**, Identification of the elbow. Long-distance cross-link midpoint density (see Fig. 2c) was mapped onto the structure. **c**, Structure of the elbow. The C-terminal coiled-coil helix is distorted (kinked) close to the conserved Tyr416 on the N-terminal helix. Residues for visual reference between the views are shown in gray. Residues targeted by mutagenesis (Supplementary Fig. 3) are highlighted in black. See also Table 1.

at a near-central position in the arm and allows the hinge of MukB to approach the head–MukEF module. Importantly, comparison of SEC profiles from native and cross-linked material suggests that native MukBEF mostly adopts a closed conformation under the conditions used (Fig. 1e).

It has been noted in previous studies that other SMC arms sometimes contain kinks[9,13,38,39]. This led us to address whether eukaryotic cohesin would also be able to adopt a defined folded conformation similar to that of MukBEF. We purified budding yeast cohesin produced in insect cells, containing Smc1, Smc3, the kleisin Scc1 and the HAWK protein Scc3, and, as for MukBEF, we stabilized the complex by mild cross-linking with BS^3 and imaged it by negative-stain EM (Fig. 1h and Supplementary Fig. 2b,c). The complex appeared in a folded conformation resembling that of MukBEF and reference-free 2D classification revealed well-resolved features in the averages. The head–kleisin–HAWK (Smc1 and Smc3 ATPase heads, Scc1, Scc3) module of cohesin is visible as a cherry-shaped density at one end of the complex. It is adjacent to a small constriction that probably represents the conserved head-proximal coiled-coil discontinuity called the 'joint'[15,19]. The cohesin hinge, which is larger than the MukB hinge, is visible as a circular density in the immediate vicinity of the joint. The cohesin elbow is located at an off-center position within the SMC arms, in contrast to MukBEF but, similar to MukBEF, allows them to bend at an angle close to 180°. We conclude that the ability to fold at an SMC elbow is shared by two very distantly related SMC–kleisin complexes.

Identification of the elbow position in MukBEF and cohesin. To ascertain where the elbow might be located at the sequence level, we used mass spectrometry to identify the BS^3-cross-linked residue pairs in both MukBEF and a cohesin complex comprising Smc1, Smc3, Scc1, Scc3 and the loader protein Scc2. We observed 176 distinct inter-subunit cross-links for MukBEF (Fig. 2a) as well as 352 additional intra-subunit cross-links, whereas analysis of cohesin identified 241 inter- and 503 intra-subunit cross-links (Supplementary Dataset 2 and Supplementary Fig. 2d). Using spatial information from crystal structures of the MukEF and the MukB head–MukF carboxy-terminal winged-helix domain (cWHD) subcomplexes[11], we computed kernel density estimates for the distribution of inter-subunit cross-links (Fig. 2b and Supplementary Fig. 2e). The distribution of observed cross-links is congruent with the position of known subunit interfaces, indicating that our cross-linking experiment faithfully reports the structure of the complex. We used the same approach to localize regions at the MukB hinge that cross-linked to head-proximal sites and the MukEF module (Supplementary Fig. 2f). Cross-links clustered at a coiled-coil region near the hinge[40], consistent with the idea that the complex folds at an elbow. To pinpoint the elbow region precisely, we next mapped all MukB coiled-coil residues onto a unified sequence coordinate system along the arm (accounting for the antiparallel nature of the SMC arm coiled coils), using available disulfide cross-linking data as a guide[41]. We then filtered intra-molecular cross-links in MukB for long-distance residue pairs in this coordinate system and determined the midpoint for each pair. If the coiled-coil arm folds at a defined elbow position, then the midpoints should reveal it, and indeed, midpoints clustered at a central region of the MukB arm (Fig. 2c). As a negative control, clustering was not observed in randomly permutated data (Supplementary Fig. 2g). Kernel density estimation produced a pronounced peak close to the 180th coiled-coil residue in the arm coordinate system (corresponding to MukB residues 427 and 970 on the N- and C-terminal coiled-coil strands, respectively).

We used a similar approach to identify the elbow's position in cohesin. As was the case for MukBEF, kernel density estimates for inter-subunit cross-links are in good agreement with available crystal structures[19,42] (Fig. 2d and Supplementary Fig. 2e). Consistent with our observations by EM (Fig. 1h), the arms of Smc1 and Smc3 both showed midpoint clustering of cross-links at a position away from the center (Fig. 2e), indicating the presence of the elbow close to residues 391 and 806 in Smc1 (coiled-coil residue 215 in the arm coordinate system) and residues 396 and 808 in Smc3 (residue 212 in the arm coordinate system). These findings suggest that cohesin's elbow is shifted towards the hinge, in contrast to MukBEF's center position (Figs. 2c and1g,h). Using the same method, we re-analyzed published cross-linking and mass-spectrometry (CLMS) data for human and budding yeast cohesin[43,44] and obtained similar results (Supplementary Fig. 2h). We conclude that although cohesin and MukBEF each contain a defined elbow that enables folding, its relative position within the SMC proteins appears to be variable around the coiled-coil midpoint.

Structure of the MukB elbow. To investigate whether the MukB arm contains structural features that would allow it to bend at the elbow position, we purified a fusion construct between matching N- and C-terminal fragments containing the elbow as determined above and solved its structure by X-ray crystallography (Fig. 3a and Table 1). Consistent with findings from disulfide cross-linking experiments, the arm contains two coiled-coil discontinuities or 'knuckles' in this region[41]. The knuckle, which has previously been named K1-2, is at a central position, joining the coiled-coil regions formed by helices α1–α7 and α2–α6. Knuckle K1-2 is followed by the K2-3a break formed by helices α3, α4 and α5. Mapping the long-distance cross-link midpoints onto the structure identifies the K1-2 break as the elbow (Figs. 2c and 3b). In the crystal, the elbow adopts an extended and gently bent conformation. It contains an 'anchor' segment in its N-terminal α1 helix, which connects to α2 via a loop (Fig. 3c). The corresponding C-terminal segment of the arm winds around the elbow anchor helix, starting at α6, which connects to α7 via a distorted helical stretch. A conserved Tyr residue (Y416) (Fig. 3c and Supplementary Fig. 3a,b) is wedged into the α6–α7 connection and possibly contributes to its distortion by obstruction with the bulky Tyr side chain. The tip of α6 forms a short interface with the anchor helix (Fig. 3c). Conceivably, unzipping of this interface might further destabilize the α6–α7 connection to allow transition of the extended elbow to a folded conformation.

Codon substitutions at the chromosomal *mukB* locus that either changed Leu960, located at the α1–α6–anchor helix interface, to Glu (L960E) or changed the central Tyr416 to Asp or Pro (Y416D and Y416P, respectively) caused a *mukB* null phenotype: mutant strains were not viable on rich media at 37 °C, despite MukB proteins' being present at wild-type levels (Supplementary Fig. 3c-e). These findings suggest that an intact elbow region is critical for MukBEF activity in vivo. Although the details of the folded conformation remain to be determined, our findings support the idea that bending of MukBEF occurs at a predetermined, structurally defined and essential coiled-coil discontinuity in its SMC arms.

Proximity of cohesin HAWK Pds5 and the hinge in vivo. A crucial question is whether the coiled coils of SMC–kleisin complexes adopt a folded conformation in vivo as well as in vitro. We reasoned that if such folding occurred at cohesin's elbow, then proximity of its hinge domain to ATPase head–proximal sequences might permit site-specific chemical cross-linking between residues within the hinge and those associated with ATPase heads. To this end, we generated yeast strains in which residues within the Smc1 hinge were substituted by the unnatural amino acid BPA (p-benzoyl L-phenylalanine) (Fig. 4a), the side chain of which can be activated by ultraviolet (UV) light to cross-link to residues in its vicinity. After UV treatment of intact cells, we immunoprecipitated cohesin and analyzed the cross-linking reaction by western blotting (Fig. 4b). An Smc1 mutant with a BPA substitution at Glu593 efficiently cross-linked to Smc3 (Fig. 4b) because this residue is positioned directly at the Smc1–Smc3 hinge interface. Strikingly, a BPA-substitution mutant of Lys620, located on the coiled-coil distal face of the hinge, efficiently cross-linked to a large protein other than Smc3. This protein was identified as the HAWK protein Pds5, which is part of the head module (Fig. 4b). We verified that BPA was incorporated into Smc1(K620BPA) (Supplementary Fig. 4) and that cross-linking between Smc1(K620BPA) and Pds5 was dependent on UV treatment (Fig. 4c). Moreover, mutation of the Pds5 binding site in Scc1 by substitution of Val137 for lysine (V137K) greatly diminished Pds5 recruitment and prevented cross-linking to the Smc1(K620BPA) hinge[45] (Fig. 4d).

At present, we cannot exclude the possibility that cross-linking between Pds5 and the Smc1 hinge occurs between two different cohesin complexes or that Pds5 can bind close to the hinge in a way that only indirectly depends on Scc1. However, if cross-linking happens within a single cohesin complex and Pds5 contacts the hinge while bound to Scc1, then this would necessitate a folded conformation similar to that observed by EM (Fig. 1h). We note that it has previously been observed that a fluorescent tag inserted into the Smc1 hinge of cohesin produces a weak FRET signal when combined with a fluorescent tag on Pds5 (ref. [46]), which is consistent with our observations. We conclude that folding of cohesin's coiled coils most probably occurs in vivo as well as in vitro.

Table 1 | Data collection and refinement statistics

	E. coli MukB elbow (PDB 6H2X)[a]
Data collection	
Space group	$P2_1$
Cell dimensions	
a, *b*, *c* (Å)	81.12, 35.04, 81.71
α, *β*, γ (°)	90.0, 93.6, 90.0
Resolution (Å)	40.8-2.6 (2.72-2.60)
R_{pim}	0.041 (0.390)
$I/\sigma(I)$	9.7 (2.0)
$CC_{1/2}$	0.998 (0.917)
Completeness (%)	99.9 (100)
Redundancy	6.5 (6.9)
Refinement	
Resolution (Å)	40.8-2.6
No. of reflections	14,583
R_{work} / R_{free}	0.243/0.297
No. of atoms	
Protein	5607
Water	4
B factors	
Protein	97.0
Water	58.0
R.m.s. deviations	
Bond lengths (Å)	0.002
Bond angles (°)	0.43

[a]The MukB elbow structure was solved from a single-crystal dataset.

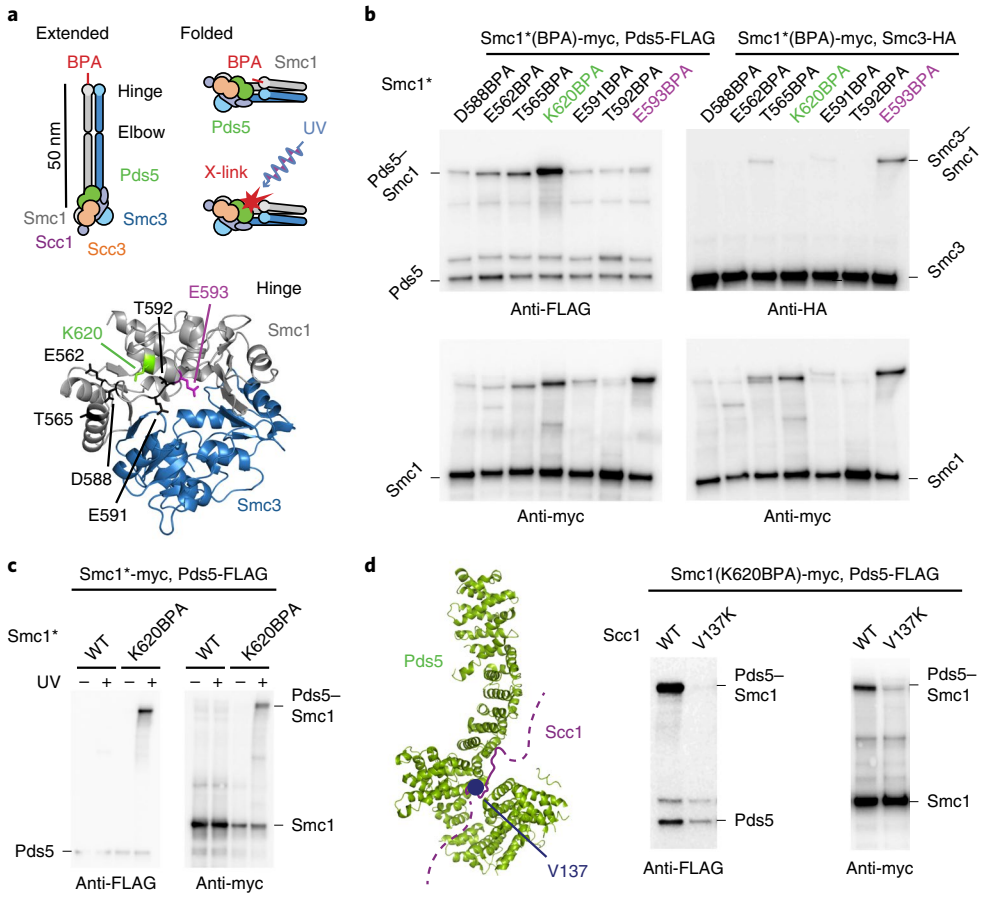

Fig. 4 | In vivo cross-linking of Pds5 to the Smc1 hinge. a, Illustration of the BPA cross-linking experiment (top) and mapping of tested BPA substitutions onto a homology model of the cohesin hinge (bottom). **b**, Screen for Smc1(BPA) cross-links to Pds5 and Smc3. BPA was incorporated into the indicated Smc1 positions, cells were treated with UV, cohesin was immunoprecipitated via a PK9-tag on Scc1 and products were analyzed by western blotting. **c**, UV-dependent cross-linking of Smc(K620BPA) and Pds5. Cells were either treated or not treated with UV and products were analyzed as in **b**. **d**, Cross-linking of Smc(K620BPA) and Pds5 depends on binding of Pds5 to Scc1. The left panel shows the position of Scc1 Val137 in its Pds5 binding site (mapped to the *Lachancea thermotolerans* structure, PDB ID 5F0O). The right panel shows a cross-linking experiment of Smc1(K620BPA) in the presence of Scc1(V137K)-PK9 as in **b**. Uncropped blots are shown in Supplementary Dataset 1.

Conservation of the SMC elbow. It has been noted before that coiled-coil prediction profiles for SMC sequences often contain a considerable drop in coiled-coil probability close to the SMC heads and often another at a more central position[47]. We wished to confirm and corroborate these findings by extending the analysis to a large set of protein sequences. We predicted coiled-coil probabilities for hundreds of individual full-length sequences using MARCOIL, extracted profiles for N- and C-terminal halves, aligned them on the arm center and averaged the profiles to remove noise (Fig. 5). The aggregate profiles for different classes of SMC proteins clearly indicate the position of a head proximal coiled-coil discontinuity, mapping it to the structurally conserved joint[15,19]. Importantly for our work, the profiles also predict the presence of a centrally located coiled-coil discontinuity in most, if not all, SMC protein families with high confidence, as judged by random resampling (Fig. 5). For MukB, the predicted central position is in excellent agreement with the elbow position estimated here experimentally by CLMS (minimum coiled-coil probability at residues 432 and 970; maximum cross-link midpoint probability density close to residues 427 and 970). These residues are located directly within the K1-2 break present in our crystal structure (Fig. 3). Similarly, the predicted elbow positions for cohesin's Smc1 and Smc3 (residues 374 and 790, and 397 and 796, respectively) are close to our experimental estimates (residues 391 and 806 and residues 396 and 808, respectively). It appears that the prediction method is accurate for the two distantly related SMC–kleisin complexes, which we have investigated here, and hence can probably be applied to other SMC proteins. In addition, the coiled coils of both bacterial and archaeal Smc proteins contain a discontinuity close to the position predicted by our aggregate profiling approach[15,47] (Supplementary Fig. 5). Interestingly, in *Bacillus subtilis* Smc this region is among the few that tolerates peptide insertions[24]. Among bacterial and archaeal Smc proteins, a predicted elbow is particularly apparent in profiles of naturally occurring short variants (Fig. 5). We conclude that a central coiled-coil discontinuity is present in most if not all classes of SMC proteins, indicating that bending at a defined elbow may be a fundamental feature.

Discussion

Conformational states and their interconversions in SMC–kleisin complexes. The first electron microscopic images of isolated SMC proteins were obtained by rotary metal shadowing of mica-adsorbed proteins and revealed a characteristic shape: positioned at the ends of a long coiled-coil arm were identified the globular hinge dimerization and head ATPase domains[9,14,16]. In these early studies, SMC dimers were largely observed as V-, I- (rod) or O-shaped particles. Furthermore, it was noticed that the SMC arms would sometimes be kinked[9,13,16,38]. Other studies employing

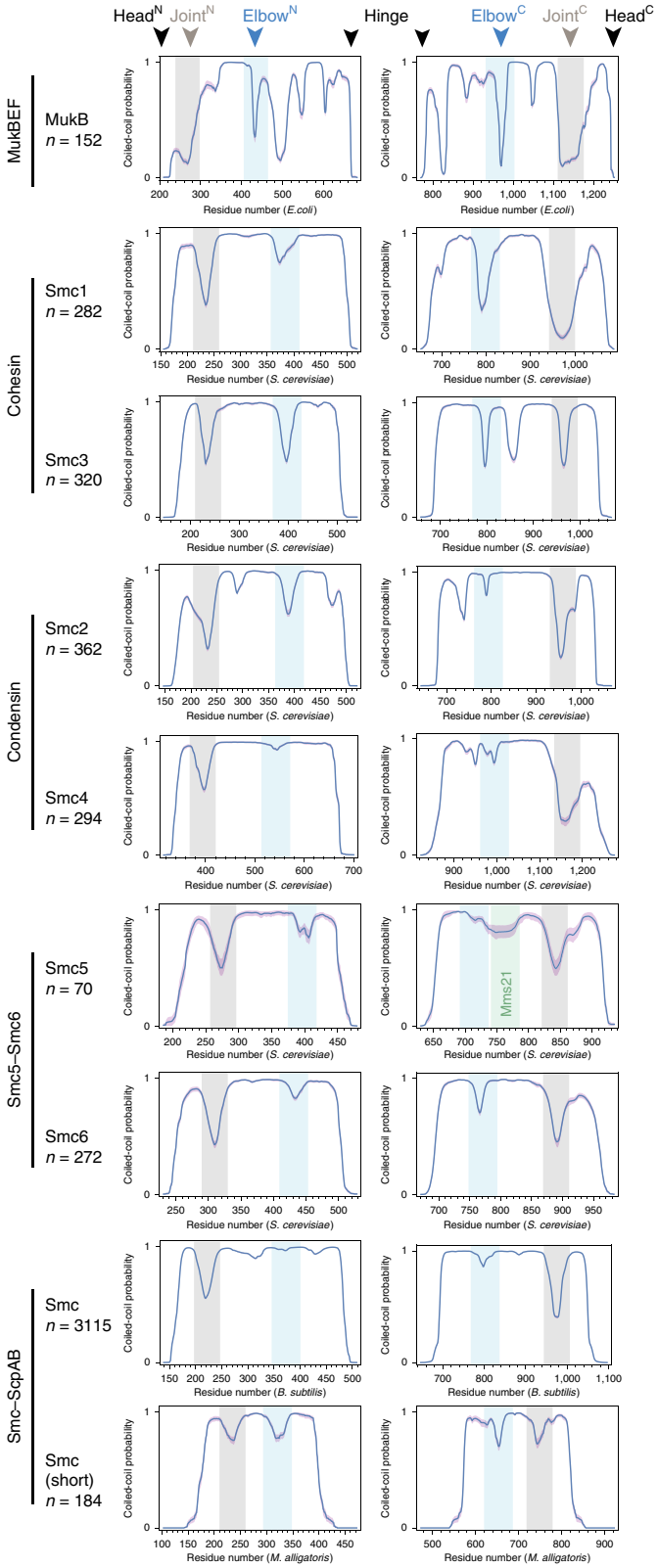

Fig. 5 | Conservation of the SMC elbow. Coiled-coil prediction profiles for a diverse set of SMC protein sequences were generated by MARCOIL. Profiles for N- and C-terminal parts of the arms were separately aligned on their center coordinate and averaged. 90% confidence intervals (purple shading) were estimated by random resampling 100 times with replacement. The Mms21 binding site of Smc5 is highlighted in green. *n*, number of sequences used for generating the respective aggregate profiles. Source data are available online.

atomic-force microscopy have suggested that isolated Smc2–Smc4 heterodimers of condensin may adopt a compact conformation[39] or may have highly flexible arms with a short persistence length[48]. The apparent presence of coiled-coil breaks within SMC arms prompted the prediction that 'the coiled coil undergoes a dramatic conformational change to allow a direct interaction between the hinge domain and the head domain or a head-proximal portion of the coiled coil'[47].

Here we demonstrate that two substantially diverged SMC–kleisin complexes, namely bacterial MukBEF and eukaryotic cohesin, are able to adopt a well-defined folded conformation that brings their hinge into proximity with their heads. Folding of the complexes occurs at a centrally positioned coiled-coil discontinuity, the 'elbow', that is present in most if not all SMC proteins. The elbow is apparent as a sharp kink also in cryo-EM images of MukBEF particles, without the use of surface immobilization, dehydration, staining or mechanical probing of the sample (Supplementary Fig. 1d), and it is detectable by in-solution cross-linking and mass spectrometry. CLMS contact sites are fully consistent with a folded state and are in excellent agreement with computational predictions for the elbow position and also crystallographic data (Figs. 2, 3, 5). Size-exclusion chromatography of *E. coli* MukBEF coupled to negative-stain EM suggests that a considerable fraction of this complex adopts a folded conformation (Fig. 1e,f). An apparently smaller fraction adopts an extended ('I' or rod) conformation, which resembles the shape of *B. subtilis* Smc–ScpAB[15,49]. Interestingly, treatment of MukBEF with the cross-linker BS^3 strongly enriches the extended rod fraction. Hence, it seems likely that MukBEF can interconvert between folded and extended forms and that reaction with BS^3 artificially triggers or traps this switch.

If MukBEF and cohesin alternate between folded and extended states, then it is conceivable that this may be coupled to their DNA binding and ATP-hydrolysis cycle. The SMC arms are firmly anchored in the ATPase heads, which would enable such coupling. In Smc–ScpAB, a link between the ATPase cycle and arm conformation is supported by site-specific cross-linking experiments, indicating a conformational change in the coiled coil upon binding of ATP and DNA[25,49]. These experiments are consistent with a disengagement of the arm–arm interface, which may convert Smc–ScpAB from a rod-like state to a ring-like state. If both folded and extended conformations interconvert in MukBEF and cohesin, we suspect that they may do so via an intermediate that accommodates considerable strain in their arms. Such an intermediate might correspond to this 'open' or ring-like state (Fig. 6a).

How could a folding and extension cycle, possibly driven by the ATPase, be implemented at the structural level? One conundrum is how an SMC dimer with a central twofold symmetry axis is able to adopt a folded state such as those observed here. Making an SMC dimer bend to one side must break this symmetry, as the symmetry dictates that the two arms bend to opposite sides if the same bending angle direction is applied to each SMC coiled coil (Supplementary Fig. 6). To bend both arms to the same side, there are two options: the monomers might bend in opposite directions within their respective body frames, or they might rotate 180° relative to each other and then bend into the same direction. The latter insight allows the construction of a simple hypothesis: conformational switching between folded and extended states might be achieved by rotating the arms against each other. This would bring the monomer elbows into an orientation that either is or is not compatible with dimer folding at the elbow, depending on the starting conformation. If such a rotation introduced or removed strain (for example, by twisting the heads during the ATPase cycle while keeping the hinges fixed), this could actively promote switching. The reader is encouraged to elaborate on these insights by building and twisting the accompanying paper model (Fig. 6b). Of note, asymmetric binding of SMC proteins by the kleisin appears to be a widely conserved

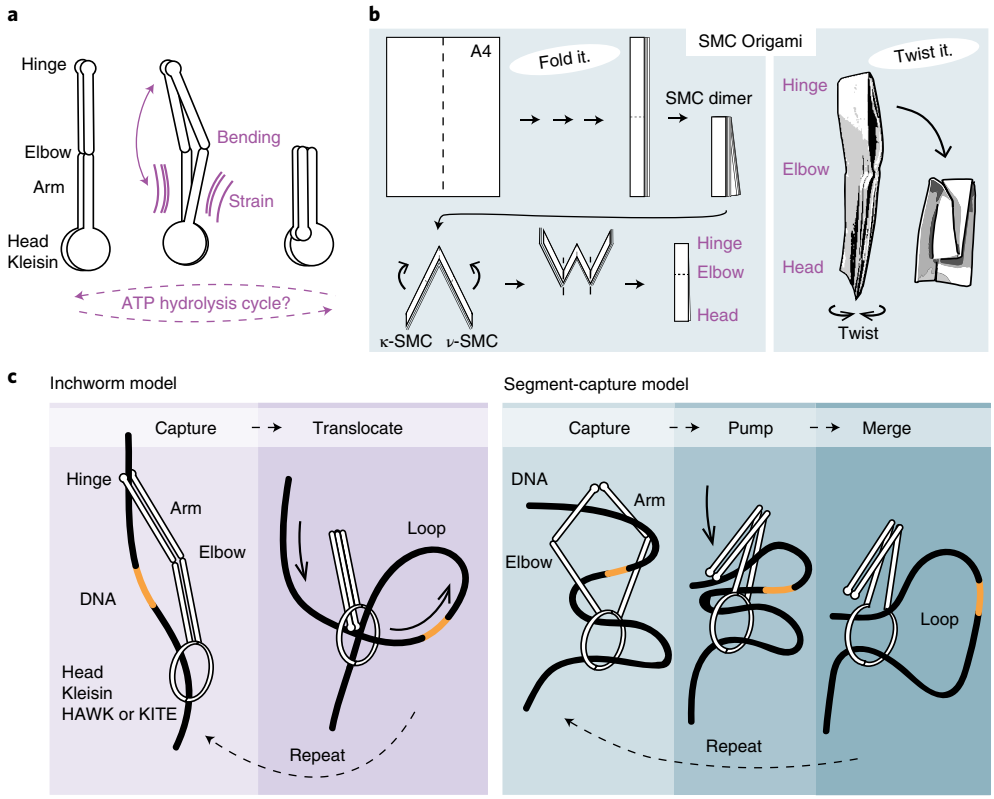

Fig. 6 | Models for conformational changes that involve the SMC elbow. a, Model for regulated conformational switching of SMC–kleisin complexes. Transitioning between extended and folded states in either direction might be driven by the ATPase cycle introducing mechanical strain into the SMC arms. **b**, Paper model. Conversion between extended and folded states is achieved by twisting the arms of the model. **c**, Models for DNA translocation and loop extrusion involving a folded state. Left, 'inchworm translocation' using distance changes between two DNA binding sites, either of which might be a topological entrapment device or ring, for example, formed by the kleisin and the SMC heads or the kleisin and its associated HAWK or KITE subunits. Folding at the elbow might cause the distance change. Right, translocation using the segment-capture mechanism that enlarges a loop held in a bottom chamber by merging with a smaller loop captured in a top chamber. Folding at the elbow might drive DNA from top to bottom.

feature and might facilitate the asymmetric twisting[9,10,12]. A robust mechanical principle such as this could be harnessed to implement folding at arbitrary positions along the arm, only depending on the position of the elbow. However, it requires heads and hinges to have particular relative angular orientations. Consistent with this idea, function of Smc–ScpAB appears to be influenced by the superhelical phase-relationship between the ends of its arms, suggesting that ATPase heads and hinges must be attached to the coiled-coil arms in fixed and pertinent relative orientations[24].

Shape transformations for DNA transactions. SMC–kleisin complexes in prokaryotes and eukaryotes appear to share three possibly overlapping activities that are likely to be central to their biological function: DNA entrapment, DNA translocation and DNA loop extrusion. How these activities are interconnected and how they are biochemically implemented remain exciting and important questions. Understanding DNA translocation appears especially relevant, because it is almost certainly required for any kind of DNA loop extrusion. Translocation on chromosomes depends on ATP hydrolysis by the SMC heads[25–28] and is probably driven by internal motor activity at least in condensin[30,31]. The SMC arms are likely to play a role in DNA loading and/or translocation, because their disruption in Smc–ScpAB largely uncouples ATP hydrolysis from entrapment of DNA and movement on chromosomes[24]. Similarly, mutations in the cohesin hinge can uncouple nucleotide hydrolysis and translocation[50]. Apart from translocation, DNA loading of cohesin has been suspected to be mediated by cross-talk between hinge and head modules[23,51]. We envision that a large-scale conformational change in the arms, such as folding at the elbow, is involved in DNA translocation or entrapment by SMC–kleisin complexes.

How might a folded conformation of SMC–kleisin complexes take part in the translocation reaction? One possibility is that switching between extended and folded conformations might change the distance between two DNA contact sites, possibly located at the ends of the SMC–kleisin rod, thereby permitting inchworm-like movement along the substrate (Fig. 6c and Supplementary Fig. 7). DNA-binding activity has been reported for the head domains of MukB, the SMC-like Rad50 and Smc–ScpAB[11,52–54]. Moreover, isolated hinge domains of cohesin, condensin, Smc5–Smc6 and Smc–ScpAB are also able to bind DNA[49,55–57]. The MukB hinge, although lacking a strong interaction with DNA, associates with the DNA-binding proteins topoisomerase IV and MatP, suggesting that it might at least come into proximity with the substrate[58,59]. Translocation via an inchworm-like mechanism would require at least one of the contact sites to act as a 'grapple'; that is, it must have regulated DNA affinity for capture and release of the substrate (Supplementary Fig. 7). The second site would act as an 'anchor', keeping the complex attached to DNA while the grapple is released. DNA binding at either site might not be purely electrostatic but may involve steric entrapment of the substrate, similar to the sliding clamp of DNA polymerase. In addition, the DNA binding sites could also be located on different complexes that act in concert, as is clearly a possibility for chromosomal MukBEF[27].

Transport of DNA within Smc–ScpAB complexes has been suggested to involve the transition from a rod-like state to a ring-like state, whereby DNA is captured between the SMC arms to be

pushed from a hinge-proximal site towards a head-proximal compartment[15,25,49,60]. Although a central coiled-coil discontinuity that is structurally unrelated to the MukB elbow is present in bacterial and archaeal Smc proteins (Fig. 5 and Supplementary Fig. 5), it is currently unclear whether these proteins are able to adopt a folded conformation at any stage of their activity cycle. Prokaryotic Smc proteins are distant relatives of both MukB and cohesin's Smc1 and Smc3, and folding might have arisen by convergent evolution of MukBEF and cohesin. In such a scenario, a central coiled-coil discontinuity or SMC elbow might have a twofold role: first, it might support bending of the relatively rigid arms into a ring or rhombus that can accommodate DNA, which might be assisted by secondary coil-coil discontinuities in MukBEF[40,41] (Fig. 3); second, transition to a folded conformation might build on top of this possibly primordial activity to provide transport directionality by pushing DNA from one end of the complex to the other (Fig. 6c). However, at present it is unclear whether DNA translocation, or loop extrusion, requires entrapment within the tripartite ring, and whether DNA entrapment requires access to the inter-arm space. In a scenario in which the essential activities of SMC complexes are performed largely by the head–kleisin module, the arms might have a regulatory role. For example, adoption of a folded conformation might adjust head arrangement by the putative twisting mechanism described above and perhaps inhibit or facilitate opening of a DNA entry or exit gate. Alternatively, folding might position hinge-associated factors, such as Topoisomerase IV[59], close to a DNA substrate bound at the head module. Given the remarkable length of the arms, and the conservation thereof, we prefer mechanical models over purely regulatory ones. Clarifying the nature of the DNA-bound states of SMC–kleisin complexes, tracking the path of the kleisin and the associated DNA, and understanding how exactly the head ATPase affects SMC–kleisin structure are now of utmost importance.

In summary, we show that the evolutionarily distant SMC–kleisin complexes MukBEF and cohesin adopt very similar folded conformations by bending at a central coiled-coil discontinuity, the elbow. We provide evidence that the elbow is a widespread feature among SMC proteins and propose that it is involved in a conformational switch that drives DNA transactions of many if not all SMC–kleisin complexes.

Online content

Any methods, additional references, Nature Research reporting summaries, source data, statements of data availability and associated accession codes are available at https://doi.org/10.1038/s41594-019-0196-z.

Received: 11 July 2018; Accepted: 25 January 2019;
Published online: 4 March 2019

References

1. Hirano, T. Condensin-based chromosome organization from bacteria to vertebrates. *Cell* **164**, 847–857 (2016).
2. Niki, H., Jaffe, A., Imamura, R., Ogura, T. & Hiraga, S. The new gene mukB codes for a 177 kd protein with coiled-coil domains involved in chromosome partitioning of E. coli. *EMBO J.* **10**, 183–193 (1991).
3. Britton, R. A., Lin, D. C. & Grossman, A. D. Characterization of a prokaryotic SMC protein involved in chromosome partitioning. *Genes Dev.* **12**, 1254–1259 (1998).
4. Saka, Y. et al. Fission yeast cut3 and cut14, members of a ubiquitous protein family, are required for chromosome condensation and segregation in mitosis. *EMBO J.* **13**, 4938–4952 (1994).
5. Michaelis, C., Ciosk, R. & Nasmyth, K. Cohesins: chromosomal proteins that prevent premature separation of sister chromatids. *Cell* **91**, 35–45 (1997).
6. Guacci, V., Koshland, D. & Strunnikov, A. A direct link between sister chromatid cohesion and chromosome condensation revealed through the analysis of MCD1 in *S. cerevisiae*. *Cell* **91**, 47–57 (1997).
7. Hirano, T. & Mitchison, T. J. A heterodimeric coiled-coil protein required for mitotic chromosome condensation in vitro. *Cell* **79**, 449–458 (1994).
8. Klein, F. et al. A central role for cohesins in sister chromatid cohesion, formation of axial elements, and recombination during yeast meiosis. *Cell* **98**, 91–103 (1999).
9. Haering, C. H., Löwe, J., Hochwagen, A. & Nasmyth, K. Molecular architecture of SMC proteins and the yeast cohesin complex. *Mol. Cell* **9**, 773–788 (2002).
10. Bürmann, F. et al. An asymmetric SMC-kleisin bridge in prokaryotic condensin. *Nat. Struct. Mol. Biol.* **20**, 371–379 (2013).
11. Woo, J. S. et al. Structural studies of a bacterial condensin complex reveal ATP-dependent disruption of intersubunit interactions. *Cell* **136**, 85–96 (2009).
12. Zawadzka, K. et al. MukB ATPases are regulated independently by the N- and C-terminal domains of MukF kleisin. *eLife* **7**, e31522 (2018).
13. Anderson, D. E., Losada, A., Erickson, H. P. & Hirano, T. Condensin and cohesin display different arm conformations with characteristic hinge angles. *J. Cell Biol.* **156**, 419–424 (2002).
14. Melby, T. E., Ciampaglio, C. N., Briscoe, G. & Erickson, H. P. The symmetrical structure of structural maintenance of chromosomes (SMC) and MukB proteins: long, antiparallel coiled coils, folded at a flexible hinge. *J. Cell Biol.* **142**, 1595–1604 (1998).
15. Diebold-Durand, M. L. et al. Structure of full-length SMC and rearrangements required for chromosome organization. *Mol. Cell* **67**, 334–347.e5 (2017).
16. Niki, H. et al. *E.coli* MukB protein involved in chromosome partition forms a homodimer with a rod-and-hinge structure having DNA binding and ATP/GTP binding activities. *EMBO J.* **11**, 5101–5109 (1992).
17. Palecek, J. J. & Gruber, S. Kite proteins: a superfamily of SMC/kleisin partners conserved across bacteria, archaea, and eukaryotes. *Structure* **23**, 2183–2190 (2015).
18. Wells, J. N., Gligoris, T. G., Nasmyth, K. A. & Marsh, J. A. Evolution of condensin and cohesin complexes driven by replacement of Kite by Hawk proteins. *Curr. Biol.* **27**, R17–r18 (2017).
19. Gligoris, T. G. et al. Closing the cohesin ring: structure and function of its Smc3-kleisin interface. *Science* **346**, 963–967 (2014).
20. Cuylen, S., Metz, J. & Haering, C. H. Condensin structures chromosomal DNA through topological links. *Nat. Struct. Mol. Biol.* **18**, 894–901 (2011).
21. Wilhelm, L. SMC condensin entraps chromosomal DNA by an ATP hydrolysis dependent loading mechanism in *Bacillus subtilis*. *eLife* **4**, e06659 (2015).
22. Gruber, S. et al. Evidence that loading of cohesin onto chromosomes involves opening of its SMC hinge. *Cell* **127**, 523–537 (2006).
23. Murayama, Y. & Uhlmann, F. DNA entry into and exit out of the cohesin ring by an interlocking gate mechanism. *Cell* **163**, 1628–1640 (2015).
24. Bürmann, F. et al. Tuned SMC arms drive chromosomal loading of prokaryotic condensin. *Mol. Cell* **65**, 861–872.e9 (2017).
25. Minnen, A. et al. Control of Smc coiled coil architecture by the ATPase heads facilitates targeting to chromosomal ParB/parS and release onto flanking DNA. *Cell Rep* **14**, 2003–2016 (2016).
26. Hu, B. et al. ATP hydrolysis is required for relocating cohesin from sites occupied by its Scc2/4 loading complex. *Curr. Biol.* **21**, 12–24 (2011).
27. Badrinarayanan, A., Reyes-Lamothe, R., Uphoff, S., Leake, M. C. & Sherratt, D. J. In vivo architecture and action of bacterial structural maintenance of chromosome proteins. *Science* **338**, 528–531 (2012).
28. Wang, X. et al. In vivo evidence for ATPase-dependent DNA translocation by the *Bacillus subtilis* SMC condensin complex. *Mol. Cell* **71**, 841–847 (2018).
29. Wang, X., Brandao, H. B., Le, T. B., Laub, M. T. & Rudner, D. Z. Bacillus subtilis SMC complexes juxtapose chromosome arms as they travel from origin to terminus. *Science* **355**, 524–527 (2017).
30. Ganji, M. et al. Real-time imaging of DNA loop extrusion by condensin. *Science* **360**, 102–105 (2018).
31. Terakawa, T. et al. The condensin complex is a mechanochemical motor that translocates along DNA. *Science* **358**, 672–676 (2017).
32. Nasmyth, K. Disseminating the genome: joining, resolving, and separating sister chromatids during mitosis and meiosis. *Annu. Rev. Genet.* **35**, 673–745 (2001).
33. Alipour, E. & Marko, J. F. Self-organization of domain structures by DNA-loop-extruding enzymes. *Nucleic Acids Res.* **40**, 11202–11212 (2012).
34. Marsden, M. P. & Laemmli, U. K. Metaphase chromosome structure: evidence for a radial loop model. *Cell* **17**, 849–858 (1979).
35. Yamazoe, M. et al. Complex formation of MukB, MukE and MukF proteins involved in chromosome partitioning in *Escherichia coli*. *EMBO J.* **18**, 5873–5884 (1999).
36. Lioy, V. S. et al. Multiscale structuring of the *E. coli* chromosome by nucleoid-associated and condensin proteins. *Cell* **172**, 771–783.e18 (2018).
37. Petrushenko, Z. M., Lai, C. H. & Rybenkov, V. V. Antagonistic interactions of kleisins and DNA with bacterial Condensin MukB. *J. Biol. Chem.* **281**, 34208–34217 (2006).
38. Hons, M. T. et al. Topology and structure of an engineered human cohesin complex bound to Pds5B. *Nat. Commun.* **7**, 12523 (2016).

39. Yoshimura, S. H. et al. Condensin architecture and interaction with DNA: regulatory non-SMC subunits bind to the head of SMC heterodimer. *Curr. Biol.* **12**, 508–513 (2002).
40. Li, Y., Schoeffler, A. J., Berger, J. M. & Oakley, M. G. The crystal structure of the hinge domain of the *Escherichia coli* structural maintenance of chromosomes protein MukB. *J. Mol. Biol.* **395**, 11–19 (2010).
41. Weitzel, C. S., Waldman, V. M., Graham, T. A. & Oakley, M. G. A repeated coiled-coil interruption in the *Escherichia coli* condensin MukB. *J. Mol. Biol.* **414**, 578–595 (2011).
42. Haering, C. H. et al. Structure and stability of cohesin's Smc1-kleisin interaction. *Mol. Cell* **15**, 951–964 (2004).
43. Chao, W. C. et al. Structure of the cohesin loader Scc2. *Nat. Commun.* **8**, 13952 (2017).
44. Huis in 't Veld, P. J. et al. Characterization of a DNA exit gate in the human cohesin ring. *Science* **346**, 968–972 (2014).
45. Chan, K. L. et al. Pds5 promotes and protects cohesin acetylation. *Proc. Natl Acad. Sci. USA* **110**, 13020–13025 (2013).
46. Mc Intyre, J. et al. In vivo analysis of cohesin architecture using FRET in the budding yeast *Saccharomyces cerevisiae*. *EMBO J.* **26**, 3783–3793 (2007).
47. Waldman, V. M., Stanage, T. H., Mims, A., Norden, I. S. & Oakley, M. G. Structural mapping of the coiled-coil domain of a bacterial condensin and comparative analyses across all domains of life suggest conserved features of SMC proteins. *Proteins* **83**, 1027–1045 (2015).
48. Eeftens, J. M. et al. Condensin Smc2-Smc4 dimers are flexible and dynamic. *Cell Rep.* **14**, 1813–1818 (2016).
49. Soh, Y. M. et al. Molecular basis for SMC rod formation and its dissolution upon DNA binding. *Mol. Cell* **57**, 290–303 (2015).
50. Srinivasan, N. et al. The cohesin ring uses its hinge to organize DNA using non-topological as well as topological mechanisms.*Cell* **173**, 1508–1519.e18 (2018).
51. Xu, X. et al. Suppressor mutation analysis combined with 3D modeling explains cohesin's capacity to hold and release DNA. *Proc. Natl Acad. Sci. USA* **115**, E4833–E4842 (2018).
52. Löwe, J., Cordell, S. C. & van den Ent, F. Crystal structure of the SMC head domain: an ABC ATPase with 900 residues antiparallel coiled-coil inserted. *J. Mol. Biol.* **306**, 25–35 (2001).
53. Liu, Y. et al. ATP-dependent DNA binding, unwinding, and resection by the Mre11/Rad50 complex. *EMBO J.* **35**, 743–758 (2016).
54. Lammens, A., Schele, A. & Hopfner, K. P. Structural biochemistry of ATP-driven dimerization and DNA-stimulated activation of SMC ATPases. *Curr. Biol.* **14**, 1778–1782 (2004).
55. Chiu, A., Revenkova, E. & Jessberger, R. DNA interaction and dimerization of eukaryotic SMC hinge domains. *J. Biol. Chem.* **279**, 26233–26242 (2004).
56. Griese, J. J., Witte, G. & Hopfner, K. P. Structure and DNA binding activity of the mouse condensin hinge domain highlight common and diverse features of SMC proteins. *Nucleic Acids Res.* **38**, 3454–3465 (2010).
57. Alt, A. et al. Specialized interfaces of Smc5/6 control hinge stability and DNA association. *Nat. Commun.* **8**, 14011 (2017).
58. Nolivos, S. et al. MatP regulates the coordinated action of topoisomerase IV and MukBEF in chromosome segregation. *Nat. Commun.* **7**, 10466 (2016).
59. Vos, S. M., Stewart, N. K., Oakley, M. G. & Berger, J. M. Structural basis for the MukB-topoisomerase IV interaction and its functional implications in vivo. *EMBO J.* **32**, 2950–2962 (2013).
60. Marko, J. F., De Los Rios, P., Barducci, A. & Gruber, S. DNA-segment-capture model for loop extrusion by structural maintenance of chromosome (SMC) protein complexes. *bioRxiv* https://www.biorxiv.org/content/10.1101/325373v2 (2018).

Acknowledgements

We are grateful to D. Ciziene for help with crystallography and M. Yu for help with X-ray data collection. We thank X. Deng, F. Coscia and G. Cannone for help with electron microscopy. We thank J. Fredens for advice on recombineering and for the gift of the *pheS*-hygR* cassette. We thank G. Fisher and D. Sherratt for help with initial complementation experiments and gift of the *neoR* marker. We thank the staff of beamline I04-1 at Diamond Light Source for assistance during crystallographic data collection. We thank S. Gruber and A. Durand for comments on the manuscript. F.B. is funded by an EMBO Long-Term Fellowship (EMBO ALTF 1151-2017). This work was funded by the Medical Research Council (U105184326 to J.L.), the Wellcome Trust (202754/Z/16/Z to J.L. and 202062/Z/16/Z to B.H.), the DFG (25065445 to J.R.), and the Wellcome Trust through a Senior Research Fellowship to J.R. (103139). The Wellcome Centre for Cell Biology is supported by core funding from the Wellcome Trust (203149).

Author contributions

F.B. and B.-G.L. purified proteins. F.B. and B.-G.L. performed electron microscopy experiments. L.S. and F.J.O. performed mass spectrometry experiments and identified cross-links. F.B. performed CLMS data analysis and bioinformatics. F.B. performed X-ray crystallography experiments. F.B. and J.L. analyzed X-ray diffraction data. F.B. constructed *E. coli* strains. T.T. constructed yeast strains and performed in vivo cross-linking experiments. S.Y. conceived the paper model. F.B. prepared the manuscript with input from all authors. J.R., B.H., K.N. and J.L. supervised the work.

Competing interests

The authors declare no competing interests.

Additional information

Supplementary information is available for this paper at https://doi.org/10.1038/s41594-019-0196-z.

Reprints and permissions information is available at www.nature.com/reprints.

Correspondence and requests for materials should be addressed to J.L.

Publisher's note: Springer Nature remains neutral with regard to jurisdictional claims in published maps and institutional affiliations.

Methods

Purification of MukBEF. Coding sequences for *E. coli* MukF, MukE and MukB (GenBank IDs NP_415442.1, NP_415443.2 and NP_415444.1) were inserted as a polycistronic expression construct into a pET-28-derived vector by Golden Gate cloning[61]. MukB was N-terminally fused to budding yeast His6-SUMO. The complex was produced in *E. coli* BL21-Gold(DE3) grown in ZYP-5052 autoinduction medium[62] at 24 °C. Purification of the complex was performed at 4 °C. Approximately 15 g cells were resuspended in 90 ml buffer IMAC (50 mM sodium phosphate, 300 mM NaCl, 20 mM imidazole, pH 7.4 at 4 °C) including RNase A, DNase I and protease inhibitors, and lysed in a high-pressure homogenizer at 172 MPa. The lysate was sonicated briefly to reduce viscosity, and cleared by centrifugation for 30 min at 96,000*g*. The extract was incubated with 25 ml NiNTA agarose (Qiagen) for 30 min. The resin was packed into a gravity flow column and washed with 80 ml IMAC buffer followed by 40 ml SENP buffer (10 mM sodium phosphate, 50 mM NaCl, 20 mM imidazole, pH 7.4 at 4 °C). The resin was resuspended in 25 ml SENP buffer containing 1 mM DTT and 1 mg GST-hSENP1 protease and incubated for 1 h to cleave off the His6-SUMO-tag. The flow-through containing the complex was collected and combined with an additional 12.5 ml wash of the column. The eluate was then loaded onto a 20 ml Heparin HP column (GE Healthcare), washed with two column volumes (CV) of buffer HA (10 mM sodium phosphate, 50 mM NaCl, pH 7.4 at 4 °C) and eluted with a 20 CV gradient into buffer HB (10 mM sodium phosphate, 1 M NaCl, pH 7.4 at 4 °C). The complex eluted in two peaks, and the low salt peak contained a prominent contaminant. The high salt peak fractions (at approximately 400 mM NaCl) were pooled and diluted with four volumes of buffer (10 mM Tris, 70 mM NaCl, pH 8.0 at 4 °C). The solution was loaded onto a 5 ml Q HP column (GE Healthcare). The column was washed with 2 CV of buffer QA (10 mM Tris, 200 mM NaCl, pH 8.0 at 4 °C) and eluted with a 20 CV gradient into buffer QB (10 mM Tris, 1 M NaCl, pH 8.0 at 4 °C). The complex eluted as a single peak at approximately 450 mM NaCl. Peak fractions were pooled, concentrated to about 10 mg ml^{-1} on a Vivaspin 100k filter (Sartorius), aliquoted, frozen in liquid nitrogen and stored at −80 °C. An aliquot of MukBEF was then thawed and injected into a Superose 6 Increase 3.2/300 column (GE Healthcare) in T200 buffer (10 mM Tris, 200 mM NaCl, pH 8.0 at 4 °C) to remove aggregates. The monomer fraction appeared stable for several days, as judged by SEC, but was used on the same day as the preparative SEC for all experiments. MukBEF from *Desulfovermiculus halophilus* (GenBank IDs WP_027370798.1, WP_027370797.1 and WP_027370796.1) was produced and purified similar to the *E. coli* complex.

Purification of MukB and MukEF and reconstitution of MukBEF complexes. MukB was produced and purified similar to the MukBEF holocomplex. MukEF was produced from a polycistronic expression vector with a His6-SUMO-tag on MukE and purified similar to the holocomplex, but omitting the Heparin step and using Sephacryl S200 as the size-exclusion resin. Complexes were reconstituted similar to the protocols of Petrushenko et al.[37] at 2 µM $MukB_2$ and 4 µM $MukE_4F_2$ in either 10 mM Tris, 40 mM NaCl, 2 mM $MgCl_2$, pH 8.0 (singlets, $MukBEF^S$) or in 10 mM Tris, 200 mM NaCl, pH 8.0 (doublets, $MukBEF^D$). Reactions were run over Superose 6 Increase in the respective reconstitution buffer and peak fractions were re-injected into Superose 6 Increase in T200 buffer.

Purification of cohesin. Cohesin expression constructs were cloned as described previously[63]. In brief, coding sequences for Smc1, Smc3, Scc1, Scc2 and Scc3 from *S. cerevisiae* (GenBank IDs NP_116647.1, NP_012461.1, NP_010281.1, NP_010466.3 and NP_012238.1) were synthesized with codon optimization for insect cell expression (Genscript). Sequences were individually cloned as Smc1, 8×His-Smc3, Scc1-2×StrepII, 2×StrepII-Scc3 and 2×StrepII-(151-1493)Scc2 into Multibac vectors, yielding Smc1-pACEbac1, 8×His-Smc3-pACEbac1, 2×StrepII-ΔN150-Scc2-pACEbac1, 2×StrepII-Scc3-pACEbac1 and Scc1-2×StrepII-pIDC. Tagged constructs contained an HRV 3C protease site (LEVLFQ/GP) in the tag linker. The vectors Smc1-pACEbac1, 8×His-Smc3-pACEbac1 and Scc1-2×StrepII-pIDC were combined through Gibson assembly and in vitro Cre-*lox* recombination yielding a transfer vector for the Smc1–Smc3–Scc1 trimer. The trimer, 2×StrepII-ΔN150-Scc2-pACEbac1 and 2×StrepII-Scc3-pACEbac1 transfer vectors were individually transformed into chemically competent DH10EmbacY cells. The purified bacmids were transfected into Sf9 cells using Fugene HD reagent (Promega), and the generated P1 viruses were infected into fresh Sf9 cells. The cells were grown in Insect XPRESS protein-free medium with L-glutamate (Lonza) at 27 °C for approximately 72 h, and the harvested cells were frozen in liquid nitrogen.

The frozen pellets of Sf9 culture were re-suspended in lysis buffer (20 mM Hepes pH 7.5, 125 mM NaCl, 1 mM TCEP, and 10% (w/v) glycerol) supplemented with DNase, RNase, 1 mM PMSF and EDTA-free protease inhibitor (cOmplete, Roche). Cells were lysed by sonication, and the lysates were clarified by ultracentrifugation at 200,000*g*. The clarified lysates were applied to Strep resin (5 ml StrepTrap, GE Healthcare) and eluted with 2 mM desthiobiotin in lysis buffer. 3C protease was added to the eluents to cleave the affinity tags and the cleavage products were further purified by anion exchange columns (HiTrap Q FF or mini Q (GE healthcare)) with buffers of QA (5 mM Tris, 100 mM NaCl, 1 mM TCEP, and 5% (w/v) glycerol, pH 8.0) and QB (50 mM Tris, 1 M NaCl, 1 mM TCEP, and 5% (w/v) glycerol, pH 8.0). The fractions were pooled, concentrated using a Vivaspin 100k filter (Sartorius). The purified trimer, NΔ150-Scc2, Scc3 proteins were then frozen in liquid nitrogen and stored at −80 °C until further use.

BS^3 cross-linking and SEC. An aliquot of MukBEF Q eluate was thawed and injected into a Superose 6 Increase 3.2/300 column (GE Healthcare) in P200 buffer (10 mM sodium phosphate, 200 mM NaCl, pH 7.4 at 4 °C). The monomer fraction was incubated for 2 h on ice at 0.4 mg ml^{-1} with or without 1 mM BS^3 and was injected into a Superose 6 Increase 3.2/300 column in T200 buffer (10 mM Tris, 200 mM NaCl, pH 8 at 4 °C). Chromatography was performed at a flow rate of 40 µl min^{-1}.

Negative-stain EM. For imaging of native MukBEF, an aliquot of Q eluate was thawed and injected into a Superose 6 Increase 3.2/300 column (GE Healthcare) in T200 buffer. The monomer fraction was reinjected, and the peak fraction applied to freshly glow-discharged EMS Cu Mesh 400 continuous carbon grids. Grids were stained with 2% uranyl acetate and imaged in a Tecnai Spirit microscope (FEI) using an Orius CCD camera at a pixel size of 3.5 Å and an electron dose of 40 e$^-$/Å^2 at 120 kV. For data collection, native MukBEF was applied to Quantifoil CuRh R2/2 Mesh 200 grids covered with a homemade continuous carbon film. The grids were stained with 2% uranyl formate and imaged on a Tecnai F30 Polara microscope (FEI) with a Falcon III detector using a pixel size of 1.72 Å, defocus of −0.5 to −1.5 µm and a total electron dose of 30 e$^-$/Å^2 at 300 kV fractionated into 46 frames.

BS^3 cross-linked MukBEF was prepared as described above and imaged on EMS Cu Mesh 400 continuous carbon grids stained with 2% uranyl formate. Data for SEC peak 1 (extended conformation) were collected on a Tecnai Spirit with an UltraScan CCD camera using a pixel size of 3.95 Å, defocus of −0.5 to −1.5 µm and an electron dose of 40 e$^-$/Å^2 at 120 kV. Data for SEC peak 2 (folded conformation) were collected on a Tecnai G2 F20 microscope (FEI) with a Falcon II detector using a pixel size of 2.08 Å and an electron dose of 30 e$^-$/Å^2 at 200 kV.

For imaging of cohesin, the purified trimer and Scc3 were mixed at a 1:1.5 molar ratio and injected into a Superose 6 Increase 3.2/300 column in P200 buffer. The tetramer fraction was incubated with 1 mM BS^3 for 2 h on ice and injected into a Superose 6 Increase 3.2/300 column in T200 buffer. Peak fractions were applied to Quantifoil CuRh R2/2 Mesh 200 grids covered with a homemade continuous carbon film and stained with 2% uranyl formate. Data were collected on a Tecnai G2 F20 with a Falcon II detector using a pixel size of 2.08 Å, defocus of −0.5 to −1.5 µm and an electron dose of 30 e$^-$/Å^2 at 200 kV.

Cryo-EM. *D. halophilus* MukBEF at 0.1 mg ml^{-1} was applied to glow-discharged Quantifoil Cu/Rh R2/2 Mesh 200 grids, blotted using a Vitrobot (FEI) and plunge frozen in liquid ethane. Particles were imaged on a Titan Krios microscope (FEI) equipped with a Volta phase plate and a Falcon III detector operating in linear mode, using a pixel size of 1.07 Å, defocus of −0.6 to −0.8 µm and a total electron dose of 100 e$^-$/Å^2 at 300 kV fractionated into 59 frames.

Image processing. For movies collected on a Falcon III detector, motion correction and dose weighting were performed with MotionCor2 (ref. [64]). The contrast transfer function (CTF) for electron micrographs was estimated with CTFFIND-4.1 (ref. [65]). Particle picking and reference-free 2D classification were performed in RELION2 (ref. [66]). Particles either were picked manually or were picked manually and also subjected to 2D classification followed by automatic picking in RELION2 using manually selected reference class average images low-pass filtered to 40 Å resolution. All micrographs are shown without CTF correction applied.

Cross-linking and mass spectrometry. For CLMS of MukBEF, aliquots of Q eluate were thawed and injected into a Superose 6 Increase 3.2/300 column (GE Healthcare) in buffer XL (20 mM Hepes, 150 mM NaCl, 5 mM $MgCl_2$, pH 7.8 at 23 °C). The monomer fractions were pooled and incubated at 0.4 mg ml^{-1} with 2.5 mM BS^3 for 2 h on ice before quenching with 20 mM ammonium bicarbonate for 30 min on ice. The sample was incubated for 2 min at 98 °C in the presence of LDS-PAGE sample buffer (Life Technologies) containing 6% 2-mercaptoethanol. Reaction products were separated on Criterion TGX 4-20% SDS-PAGE gels (BioRad).

For CLMS of cohesin, the purified trimer, NΔ150-Scc2 and Scc3 were mixed at a 1:1.5:1.5 ratio and injected into a Superose 6 Increase 3.2/300 column in buffer (20 mM Hepes, 150 mM NaCl and 1 mM TCEP, pH 7.7). Pentamer fractions were incubated at 2 mg ml^{-1} with 5 mM BS^3 for 2 h at 4 °C and then the reaction was quenched with 50 mM ammonium bicarbonate for 45 min on ice. Reaction products were separated on a Criterion TGX 4-15% SDS-PAGE gel (BioRad).

Gel bands corresponding to the cross-linked species were excised and digested with trypsin (Pierce). The resulting tryptic peptides were extracted and desalted using C18 StageTips[67].

For MukBEF, peptides eluted from StageTips were dried in a Vacuum Concentrator (Eppendorf) and dissolved in running buffer A prior to strong cation exchange chromatography (100 × 2.1 mm Poly Sulfoethyl A column; Poly LC). Mobile phase A consisted of 30% (v/v) acetonitrile, 10 mM KH_2PO_4 at pH 3, and mobile phase B additionally contained 1 M KCl. The separation of the digest used a non-linear gradient[68] at a flow rate of 200 µl min^{-1}. Five fractions at 2 min in the high-salt range were collected and cleaned by StageTips for subsequent LC-MS/MS (liquid chromatography–tandem mass spectrometry) analysis. For cohesin,

peptides were fractionated on an ÄKTA Pure system (GE Healthcare) using a Superdex Peptide 3.2/300 (GE Healthcare) at a flow rate of 10 µl min^{-1} using 30% (v/v) acetonitrile and 0.1% (v/v) trifluoroacetic acid as mobile phase. Five 50 µl fractions were collected and dried.

Samples for analysis were resuspended in 0.1% (v/v) formic acid 1.6% (v/v) acetonitrile. LC-MS/MS analysis was conducted in duplicate for SEC fractions and triplicate for SCX fractions, performed on an Orbitrap Fusion Lumos Tribrid mass spectrometer (Thermo Fisher Scientific) coupled on-line with an Ultimate 3000 RSLCnano system (Dionex, Thermo Fisher Scientific). The sample was separated and ionized by a 50 cm EASY-Spray column (Thermo Fisher Scientific). Mobile phase A consisted of 0.1% (v/v) formic acid and mobile phase B of 80% (v/v) acetonitrile with 0.1% (v/v) formic acid. A flow-rate of 0.3 µl min^{-1} was used with gradients optimized for each chromatographic fraction from offline fractionation ranging from 2% mobile phase B to 45% mobile phase B over 90 min, followed by a linear increase to 55% and 95% mobile phase B in 2.5 min. The MS data were acquired in data-dependent mode using the top-speed setting with a 3 s cycle time. For every cycle, the full scan mass spectrum was recorded in the Orbitrap at a resolution of 120,000 in the range of 400 to 1,600 m/z. Ions with a precursor charge state between +3 and +6 were isolated and fragmented. Fragmentation by higher-energy collisional dissociation (HCD) used a decision tree logic with optimized collision energies[69]. The fragmentation spectra were then recorded in the Orbitrap with a resolution of 30,000. Dynamic exclusion was enabled with single repeat count and 60 s exclusion duration.

The fragment spectra peak lists were generated from the raw mass spectrometric data using msConvert[70] (v 3.0.11729) with default settings. A recalibration of the precursor m/z was conducted based on high-confidence (<1% FDR) linear peptide identifications, using an in-house script[71]. The recalibrated peak lists were searched against the sequences and the reversed sequences (as decoys) of cross-linked peptides using the Xi software suite[72] (v 1.6.739) (https://github.com/Rappsilber-Laboratory/XiSearch) for identification. The following parameters were applied for the search: MS1 accuracy of 3 ppm; MS2 accuracy of 10 ppm; trypsin as the enzyme (with full tryptic specificity), allowing up to four missed cleavages; BS^3 as the cross-linker (with an assumed reaction specificity for lysine, serine, threonine, tyrosine and protein N termini); carbamidomethylation on cysteine as fixed modification; and oxidation on methionine, hydrolysed or aminolysed BS^3 from reaction with ammonia or water on a free cross-linker end as variable modifications. The identified candidates were filtered to 5% FDR on link level using XiFDR[73]. CLMS data are available as Supplementary Dataset 2.

Analysis of cross-links. For mapping of contact sites, kernel density estimation was performed on a per-protein basis for the C-alpha coordinates of cross-link residue pairs present in the respective structures. The coordinates were convolved with a 3D Gaussian kernel (bandwidth, 25 Å), and the resulting probability density distributions were sampled at all C-alpha coordinates of the respective proteins.

For the determination of long-distance cross-link midpoints, we first mapped each residue onto a unified coordinate system along the arm (running from the head at coordinate 0 to the hinge at coordinate 1). Using this approach, residues that are at the same position along the coiled-coil axis but reside on opposite coiled-coil helices map to the same coordinate. For MukB, we used the coiled-coil register established by disulfide cross-linking[41] to build a piecewise linear interpolation function for the coordinate transformation. For each arm segment with a length mismatch between N- and C-terminal parts we used the shorter part as the length of the segment. Residues located in the head were mapped to coordinate 0, residues in the hinge were mapped to 1, and residues located on either the N- or C-terminal arm helix were mapped to the interval (0, 1) according to the disulfide cross-linking data. We used the same approach for cohesin but with single interval interpolation for the N- and C-terminal helices, due to the mostly unknown coiled-coil register. Finally, coordinates were scaled to an arm length in amino acids given by the sum of the individual arm segments (MukB, 365 amino acids (aa); Smc1–Smc3, 323 aa). Cross-link residue pairs with coordinates transformed according to this procedure were filtered for distances of at least 100 aa, and the corresponding midpoints were determined. Kernel density estimation for the distribution of midpoints was performed by convolution with a Gaussian kernel (bandwidth, 10 aa).

Purification of the MukB elbow fragment. Residues 333–526 of MukB (GenBank ID NP_415444.1) were fused to residues 893–1053 using an SGGS linker. The construct contained a C-terminal GSHHHHHH tag and was inserted into a pET-16 derived vector by Golden Gate cloning[61]. Selenomethionine (SeMet) labeled protein was produced in *E. coli* BL21-Gold(DE3) grown in autoinduction medium[62] PASM-5052 at 24 °C. Purification was performed at 4 °C. Approximately 40 g of cells were resuspended in 200 ml buffer NA (50 mM sodium phosphate, 300 mM NaCl, 40 mM imidazole, 1 mM DTT, pH 7.4 at 4 °C) containing DNase I, RNase A and protease inhibitors. Cells were lysed in a high-pressure homogenizer at 172 MPa, the lysate was briefly sonicated to reduce viscosity, and was cleared by centrifugation at 96,000*g* for 30 min. The extract was passed over a 5 ml HisTrap HP column (GE Healthcare), the column was washed in 10 CV NA and eluted with buffer NB (40 mM sodium phosphate, 240 mM NaCl, 400 mM imidazole, 1 mM DTT, pH 7.4 at 4 °C). The eluate was diluted in two volumes of buffer (10 mM Tris, 1 mM TCEP, pH 8.0 at 4 °C) and loaded onto a 5 ml Q HP column (GE Healthcare). The column was washed with 3 CV of buffer QA (10 mM Tris, 100 mM NaCl, 1 mM TCEP, pH 8.0 at 4 °C) and eluted with a 20 CV gradient into buffer QB (10 mM Tris, 1 M NaCl, 1 mM TCEP, pH 8.0 at 4 °C). Peak fractions were pooled and concentrated in a Vivaspin 10k filter (Sartorius) to about 10 ml before injection into a Sephacryl S200 26/60 column (GE Healthcare) in buffer SEC (10 mM Tris, 150 mM NaCl, 1 mM EDTA, 1 mM TCEP, 1 mM NaN_3, pH 7.4 at 23 °C). Peak fractions were pooled, concentrated to 21 mg ml^{-1} in a Vivaspin 10k filter, aliquoted, frozen in liquid nitrogen and stored at −80 °C. The construct had lost its N-terminal methionine, as judged by ESI-TOF mass spectrometry.

Crystallization of the MukB elbow fragment and structure determination. An aliquot of the MukB elbow construct was thawed and exchanged into buffer X (10 mM Mes, 150 mM NaCl, 1 mM EDTA, 1 mM TCEP, 1 mM NaN_3, pH 6.5 at 23 °C) using a Zeba Spin column (Thermo Scientific). Crystallization conditions were found by screening a set of 1728 conditions using an in-house robotic setup[74]. Crystals grew as thin plates at 19 °C in sitting drops with mother liquor ML1 (22% PEG 3350, 0.25 M sodium thiocyanate) or mother liquor ML2 (23.5% PEG 3350, 2% PEG 4000, 0.375 M sodium thiocyanate). Crystals mounted in nylon loops were dipped into cryoprotectant solution (23% PEG 3350, 0.257 M sodium thiocyanate, 30% glycerol in buffer X) before freezing in liquid nitrogen. X-ray diffraction data were collected at Diamond Light Source I04-1 at 100 K and a wavelength of 0.91587 Å. Several crystals were tested. A crystal grown in ML1 diffracted to the highest resolution (2.6 Å) but produced only weak anomalous signal. A crystal grown in ML2 diffracted to about 3.0 Å and yielded good anomalous signal ($I/\sigma I = 16.1$, anomalous correlation = 0.437, anomalous multiplicity = 3.5, anomalous completeness = 99.3%, $R_{pim} = 0.031$). The space group of the crystals was determined as $P2_1$ using Pointless[75]. Diffraction data were integrated with XDS[76], scaled and merged with Aimless[75], and converted to structure factor amplitudes with Ctruncate[75]. Automated structure solution with CRANK2 (ref. [77]) using data from the ML2 crystal yielded an almost complete initial model. This was used as a search model for molecular replacement in Phaser AutoMR[78] with the ML1 dataset. A random set of 5% of the reflections was retained for validation, and the model was rebuilt from scratch using Buccaneer[79]. The model was iteratively refined by manual building in Coot[80] and reciprocal space refinement using REFMAC5 (ref. [81]). At later stages, manual building was alternated with reciprocal and real space refinement using Phenix.refine[82]. Data collection and refinement statistics are listed in Table 1. The final model covers 96% of the sequence, with 97.4% of residues in the favored and 0.3% in the disallowed Ramachandran regions. The model has a MolProbity score of 1.14 (100th percentile).

***E. coli* strain construction and growth.** *E. coli* strains are based on MG1655 (DSM 18039). All chromosomal modifications were carried out by λ-Red recombineering using a temperature-sensitive plasmid carrying the λ phage genes *exo*, *bet* and *gam* under control of the heat-labile CI857 repressor[83]. A *neoR* coding sequence was joined with a transcription terminator and homology sequences by Golden Gate assembly[61] and the reaction product was integrated downstream of the chromosomal *mukFEB* terminator. An in-frame deletion of *mukB* and a *mukB-HaloTag* allele were constructed similarly, terminated by the *mukFEB* terminator and linked to the *neoR* cassette downstream of the operon. For construction of marker-free strains carrying point mutations in *mukB*, target regions were first replaced by a cassette containing the counter-selection marker *pheS(T251A, A294G)*[84] linked to a *hygR* selection marker. The cassette was then ejected by recombination with a PCR product containing the point mutation and counter-selection on media containing 2.5 mM 4-chlorophenylalanine. Strains with a *mukB* null phenotype were grown on LB (lysogeny broth) or TYE at 22 °C or on M9 (lacking thiamine) at 37 °C. Recombineering plasmids were cured in either LB at 37 °C (functional *mukB* alleles) or in M9 (lacking thiamine) at 37 °C (*mukB* null alleles). Strains were single-colony purified and verified by marker analysis, PCR and Sanger sequencing. Strains are listed in Supplementary Table 1. Phenotypic analysis was performed by streaking on TYE and growth at 37 °C for 13 h.

***E. coli* HaloTag labeling.** Cells were grown to stationary phase in LB at 22 °C, diluted in LB to optical density at 600 nm (OD_{600}) = 0.02, and grown to OD_{600} = 0.3–0.4 at 37 °C (non-permissive temperature). Cultures were mixed with 30% (w/v) ice and harvested by centrifugation. Cells were resuspended in B-PER (Thermo Fisher) containing 1 mM EDTA (pH 7.4), 5 µM HaloTag-TMR substrate (Promega), Ready-Lyse lysozyme (Epicentre), Benzonase (Sigma), protease inhibitor cocktail (Roche) and 28 mM 2-mercaptoethanol. Samples were incubated for 10 min at 37 °C, mixed with LDS sample buffer (Thermo Fisher), incubated at 95 °C for 5 min and resolved by SDS-PAGE. Gels were scanned on a Typhoon imager (GE Healthcare) using a Cy3 filter setup, and subsequently stained with InstantBlue (Expedeon).

Yeast strain construction. Smc1-myc9 with its endogenous promoter was cloned into the LEU2 2µ plasmid YEplac181 and the codon for E620 was replaced with the amber codon TAG. The TRP1 2µ pBH61 expressing the *E. coli* nonsense suppressor tRNA and tRNA synthetase system was a gift from Steven Hahn's laboratory. The endogenous Scc1 and Pds5 were fused to 9×PK and 6×FLAG epitope tags at their

C terminus, respectively. All strains are derived from the W303 background and are listed in Supplementary Table 1.

In vivo photo cross-linking. The yeast stains bearing the TAG-substituted Smc1-myc9 plasmid and pBH61 were grown in −Trp −Leu SD medium containing 1 mM BPA. Cells were collected and resuspended in 1 ml of ice-cold PBS buffer. The cell suspension was then placed in a Spectrolinker XL-1500a (Spectronics) and irradiated at 360 nm for 2 × 5 min. Extracts were prepared as described previously[26] and 5 mg of protein were incubated with 5 µl of Anti-PK antibody (Bio-Rad) for 2 h at 4 °C. Next, 50 µl of Protein G Dynabeads (Life Technology) were added and incubated overnight at 4 °C to immunoprecipitate Scc1. After washing five times with lysis buffer the beads were boiled in 2× SDS-PAGE buffer. Samples were run on a 3–8% Tris-acetate gel (Life Technology) for 3.5 h at 150 V. For western blot analysis, Anti-Myc (Millipore) and Anti-FLAG (Sigma) antibodies were used to probe for Smc1 and Pds5, respectively.

Coiled-coil predictions and conservation analysis. A set of SMC sequences and their domain delineations[24] were used for coiled-coil prediction analysis. Individual coiled-coil probability profiles were generated with MARCOIL[85], and both N- and C-terminal regions were extracted. N- and C-terminal profiles were separately aligned on their arm center coordinates, zero padded and averaged. We estimated 90% confidence intervals for the averaged profiles using the 5% and 95% quantiles of 100 identically processed sequence sets generated by random resampling with replacement.

For conservation analysis, MukB sequences were aligned using MSAProbs[86]. Jensen–Shannon divergences were computed for each alignment column according to Capra et al.[87], but using equal weights at positions with more than 30% gaps.

Statistics and reproducibility. Experiments were performed independently with similar results for the following number of times: ten times (Fig. 1a), 21 times using four different protein preparations (Fig. 1b, MukBEF), once (Fig. 1b, MukB), once (Fig. 1b, MukEF), eight times using four different protein preparations (Fig. 1e, d), three times (Fig. 1d), three times (Fig. 1e, f), once (Fig. 1g, data collection and 2D class averaging of peak 1), twice (Fig. 1g, data collection and 2D class averaging of peak 2), four times (Fig. 1h, negative-stain sample preparation and imaging), once (Fig. 1h, data collection and 2D class averaging), once (Fig. 2, CLMS of MukBEF), once (Fig. 2, CLMS of cohesin), once (Fig. 3), four times (Fig. 4b), twice (Fig. 4e), twice (Fig. 4d), once (Supplementary Fig. 1a), twice (Supplementary Fig. 1b), once with similar results from sample screening (Supplementary Fig. 1d), once with similar results under slightly altered conditions (Supplementary Fig. 2a, reconstitution), three times (Supplementary Fig. 2b), once (Supplementary Fig. 2c), twice with two independent clones each (Supplementary Fig. 3c), twice (Supplementary Fig. 3d), twice (Supplementary Fig. 3e), twice (Supplementary Fig. 4).

Reporting Summary. Further information on research design is available in the Nature Research Reporting Summary linked to this article.

Code availability

The Xi software suite is available at https://github.com/Rappsilber-Laboratory/XiSearch. Custom code for statistical analysis is available upon request.

Data availability

Crystallographic structure factors and model coordinates have been deposited in the Protein Data Bank (PDB) with accession code 6H2X. The mass spectrometry proteomics data have been deposited at the ProteomeXchange Consortium via the PRIDE partner repository[88] with the dataset identifiers PXD012370 (MukBEF) and PXD012377 (cohesin). Source data for Fig. 5 are available with the paper online. Other data are available upon request.

References

61. Engler, C., Kandzia, R. & Marillonnet, S. A one pot, one step, precision cloning method with high throughput capability. *PLoS ONE* **3**, e3647 (2008).
62. Studier, F. W. Protein production by auto-induction in high density shaking cultures. *Protein Expr. Purif.* **41**, 207–234 (2005).
63. Petela, N. J. et al. Scc2 is a potent activator of cohesin's ATPase that promotes loading by binding Scc1 without Pds5. *Mol. Cell* **70**, 1134–1148.e7 (2018).
64. Zheng, S. Q. et al. MotionCor2: anisotropic correction of beam-induced motion for improved cryo-electron microscopy. *Nat. Methods* **14**, 331–332 (2017).
65. Rohou, A. & Grigorieff, N. CTFFIND4: fast and accurate defocus estimation from electron micrographs. *J. Struct. Biol.* **192**, 216–221 (2015).
66. Fernandez-Leiro, R. & Scheres, S. H. W. A pipeline approach to single-particle processing in RELION. *Acta Crystallogr. D Struct. Biol.* **73**, 496–502 (2017).
67. Rappsilber, J., Ishihama, Y. & Mann, M. Stop and go extraction tips for matrix-assisted laser desorption/ionization, nanoelectrospray, and LC/MS sample pretreatment in proteomics. *Anal. Chem.* **75**, 663–670 (2003).
68. Chen, Z. A. et al. Architecture of the RNA polymerase II-TFIIF complex revealed by cross-linking and mass spectrometry. *EMBO J.* **29**, 717–726 (2010).
69. Kolbowski, L., Mendes, M. L. & Rappsilber, J. Optimizing the parameters governing the fragmentation of cross-linked peptides in a tribrid mass spectrometer. *Anal. Chem.* **89**, 5311–5318 (2017).
70. Chambers, M. C. et al. A cross-platform toolkit for mass spectrometry and proteomics. *Nat. Biotechnol.* **30**, 918–920 (2012).
71. Lenz, S., Giese, S. H., Fischer, L. & Rappsilber, J. In-search selection of monoisotopic peaks improves the identification of cross-linked peptides. preprint at *bioRxiv* (2018).
72. Giese, S. H., Fischer, L. & Rappsilber, J. A study into the collision-induced dissociation (CID) behavior of cross-linked peptides. *Mol. Cell Proteomics* **15**, 1094–1104 (2016).
73. Fischer, L. & Rappsilber, J. Quirks of error estimation in cross-linking/mass spectrometry. *Anal. Chem.* **89**, 3829–3833 (2017).
74. Stock, D., Perisic, O. & Lowe, J. Robotic nanolitre protein crystallisation at the MRC Laboratory of Molecular Biology. *Prog. Biophys. Mol. Biol.* **88**, 311–327 (2005).
75. Evans, P. R. & Murshudov, G. N. How good are my data and what is the resolution? *Acta Crystallogr. D Biol. Crystallogr.* **69**, 1204–1214 (2013).
76. Kabsch, W. XDS. *Acta Crystallogr. D Biol. Crystallogr.* **66**, 125–132 (2010).
77. Winn, M. D. et al. Overview of the CCP4 suite and current developments. *Acta Crystallogr. D Biol. Crystallogr.* **67**, 235–242 (2011).
78. Bunkoczi, G. et al. Phaser.MRage: automated molecular replacement. *Acta Crystallogr. D Biol. Crystallogr.* **69**, 2276–2286 (2013).
79. Cowtan, K. The Buccaneer software for automated model building. 1. Tracing protein chains. *Acta Crystallogr. D Biol. Crystallogr.* **62**, 1002–1011 (2006).
80. Emsley, P. & Cowtan, K. Coot: model-building tools for molecular graphics. *Acta Crystallogr. D Biol. Crystallogr.* **60**, 2126–2132 (2004).
81. Murshudov, G. N. et al. REFMAC5 for the refinement of macromolecular crystal structures. *Acta Crystallogr. D Biol. Crystallogr.* **67**, 355–367 (2011).
82. Afonine, P. V. et al. Towards automated crystallographic structure refinement with phenix.refine. *Acta Crystallogr. D Biol. Crystallogr.* **68**, 352–367 (2012).
83. Datta, S., Costantino, N. & Court, D. L. A set of recombineering plasmids for gram-negative bacteria. *Gene* **379**, 109–115 (2006).
84. Miyazaki, K. Molecular engineering of a PheS counterselection marker for improved operating efficiency in *Escherichia coli*. *Biotechniques* **58**, 86–88 (2018).
85. Delorenzi, M. & Speed, T. An HMM model for coiled-coil domains and a comparison with PSSM-based predictions. *Bioinformatics* **18**, 617–625 (2002).
86. Liu, Y., Schmidt, B. & Maskell, D. L. MSAProbs: multiple sequence alignment based on pair hidden Markov models and partition function posterior probabilities. *Bioinformatics* **26**, 1958–1964 (2010).
87. Capra, J. A. & Singh, M. Predicting functionally important residues from sequence conservation. *Bioinformatics* **23**, 1875–1882 (2007).
88. Vizcaino, J. A. et al. 2016 update of the PRIDE database and its related tools. *Nucleic Acids Res.* **44**, 11033 (2016).

nature structural & molecular biology

SUPPLEMENTARY INFORMATION

https://doi.org/10.1038/s41594-019-0196-z

In the format provided by the authors and unedited.

A folded conformation of MukBEF and cohesin

Frank Bürmann[1], Byung-Gil Lee[1], Thane Than[2], Ludwig Sinn[3], Francis J O'Reilly[3], Stanislau Yatskevich[4,6], Juri Rappsilber[3,5], Bin Hu[2], Kim Nasmyth[4] and Jan Löwe[1]*

[1]MRC Laboratory of Molecular Biology, Cambridge, UK. [2]Department of Molecular Biology and Biotechnology, University of Sheffield, Sheffield, UK. [3]Bioanalytics, Institute of Biotechnology, Technische Universität Berlin, Berlin, Germany. [4]Department of Biochemistry, University of Oxford, Oxford, UK. [5]Wellcome Centre for Cell Biology, University of Edinburgh, Edinburgh, UK. [6]Present address: MRC Laboratory of Molecular Biology, Cambridge, UK.
*e-mail: jyl@mrc-lmb.cam.ac

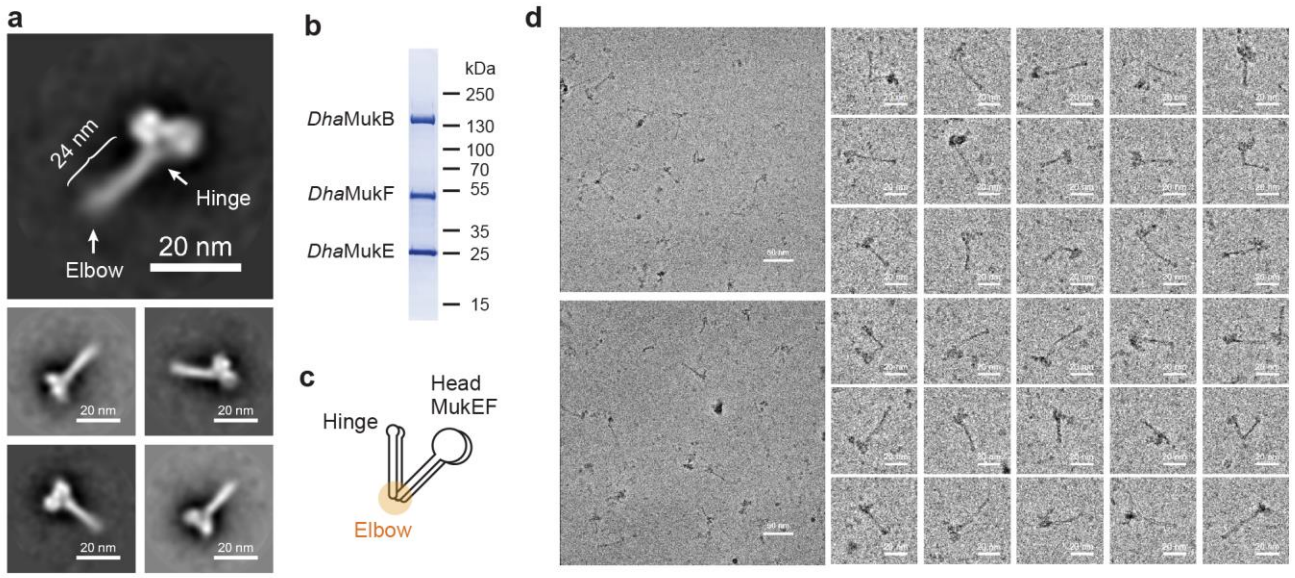

Supplementary Figure 1

EM analysis of MukBEF.

a, Negative stain 2D class averages for the folded conformation of native *E. coli* MukBEF using a circular mask of 640 Å. **b**, SDS-PAGE analysis of purified *Desulfovermiculus halophilus* MukBEF. The gel was stained with Coomassie. **c**, Cartoon of intermediate particle shapes of *D. halophilus* MukBEF indicating the presence of a coiled-coil elbow in different conformations. **d**, Cryo-EM imaging of *D. halophilus* MukBEF in unsupported vitreous ice. Contrast was enhanced by use of a Volta phase plate and high total electron dose. Typical fields of view are shown on the left, examples of single particle images are shown on the right. We estimate that approximately 35 % of particles may adopt a fully folded conformation under the conditions used. Low particle abundance and sample heterogeneity prevented further structural analysis.

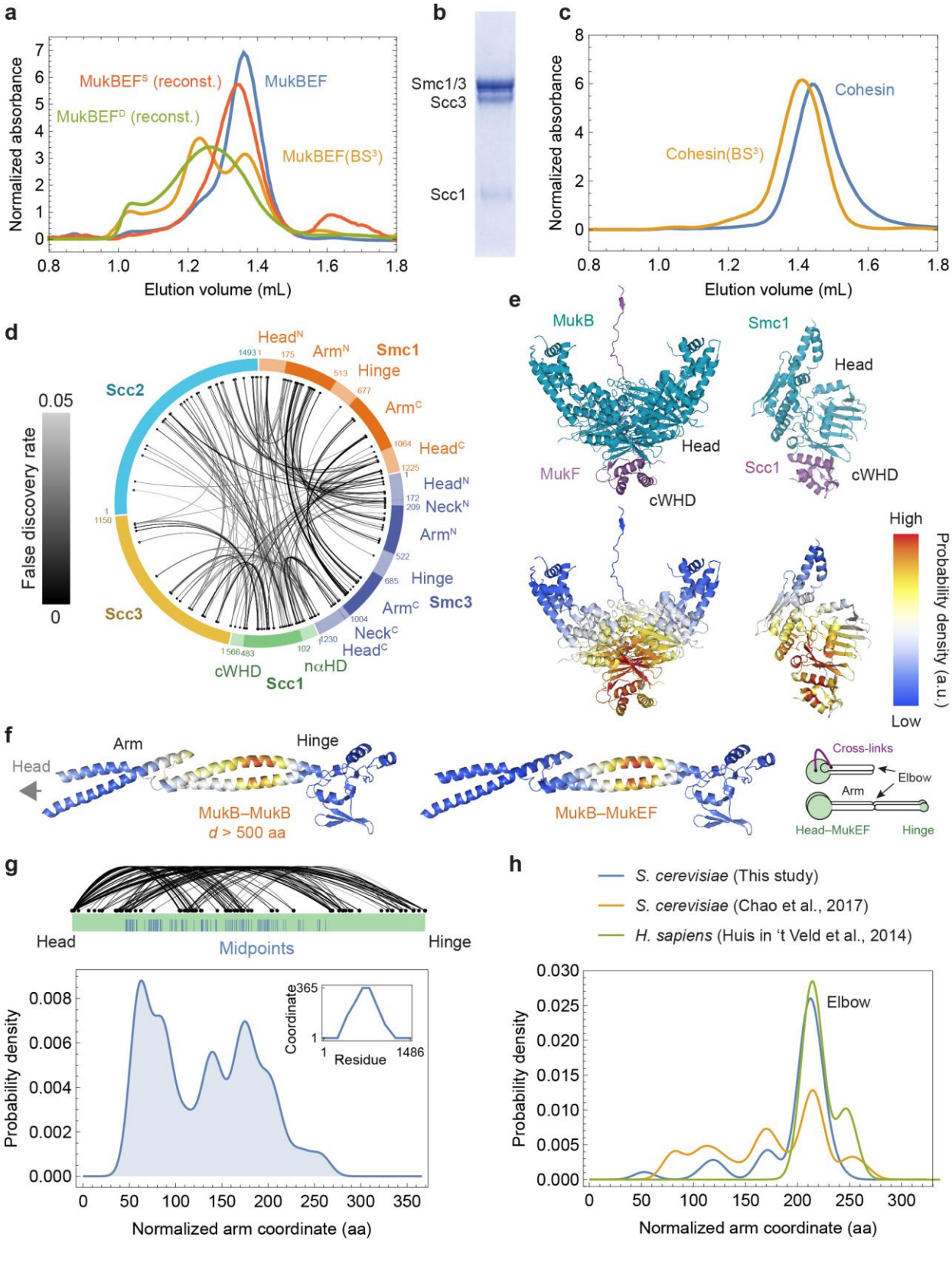
a
Normalized absorbance
Elution volume (mL)
MukBEF^S (reconst.)
MukBEF
MukBEF^D (reconst.)
MukBEF(BS^3)
b
Smc1/3
Scc3
Scc1
c
Normalized absorbance
Elution volume (mL)
Cohesin
Cohesin(BS^3)
d
False discovery rate
0.05
0
Head^N
Arm^N
Smc1
Hinge
Arm^C
Head^C
Head^N
Neck^N
Arm^N
Hinge
Arm^C
Smc3
Neck^C
Head^C
nαHD
Scc1
cWHD
Scc3
Scc2
e
MukB
Smc1
Head
Head
MukF
Scc1
cWHD
cWHD
High
Low
Probability density (a.u.)
f
Arm
Hinge
Head
MukB–MukB
d > 500 aa
MukB–MukEF
Cross-links
Elbow
Arm
Head–MukEF
Hinge
g
Head
Midpoints
Hinge
Probability density
Coordinate
Residue
Normalized arm coordinate (aa)
h
S. cerevisiae (This study)
S. cerevisiae (Chao et al., 2017)
H. sapiens (Huis in 't Veld et al., 2014)
Probability density
Elbow
Normalized arm coordinate (aa)

Supplementary Figure 2

Cross-linking and mass spectrometry of MukBEF and cohesin.

a, SEC profiles of native co-expressed MukBEF (blue), BS^3 treated co-expressed MukBEF (orange), singlet MukBEF ($MukBEF^S$) reconstituted in buffer containing 40 mM NaCl, 2 mM $MgCl_2$ (red) and doublet MukBEF ($MukBEF^D$) reconstituted in buffer containing 200 mM NaCl (green). Reconstitution was similar to protocols established previously (*J. Biol. Chem*. **281**, 34208–34217, 2006). **b**, SDS-PAGE analysis of a purified cohesin complex containing Smc1, Smc3, Scc1 and Scc3. The gel was stained with Coomassie. **c**, SEC profiles of the cohesin complex containing Smc1, Smc3, Scc1 and Scc3 before and after treatment with BS^3 (see Fig. 1h). **d**, Inter-subunit cross-links of a cohesin complex containing Smc1, Smc3, Scc1, Scc3 and Scc2. As in Fig. 2a. **e**, Kernel density estimates for the position of cross-link sites mapped onto the partial structure of the *H. ducreyi* MukBEF head module (PDB ID 3EUH) and the cohesin Smc1–Scc1 cWHD interface (PDB ID 1W1W). **f**, Kernel density estimates for long-distance cross-links at the MukB hinge. Probability density for MukB cross-links to MukB sites located at least 500 aa away (left) or to MukEF (middle). The cartoon (right) illustrates an explanation for the observed cross-linking pattern. **g**, Cross-link midpoint analysis for MukB performed as in Fig. 2c but using random resampling without replacement before data processing. **h**, Cross-link midpoint analysis for various cohesin datasets (as in Fig. 2). Peak density for human cohesin corresponds to residues 375 and 813 (Smc1) and 379 and 811 (Smc3).

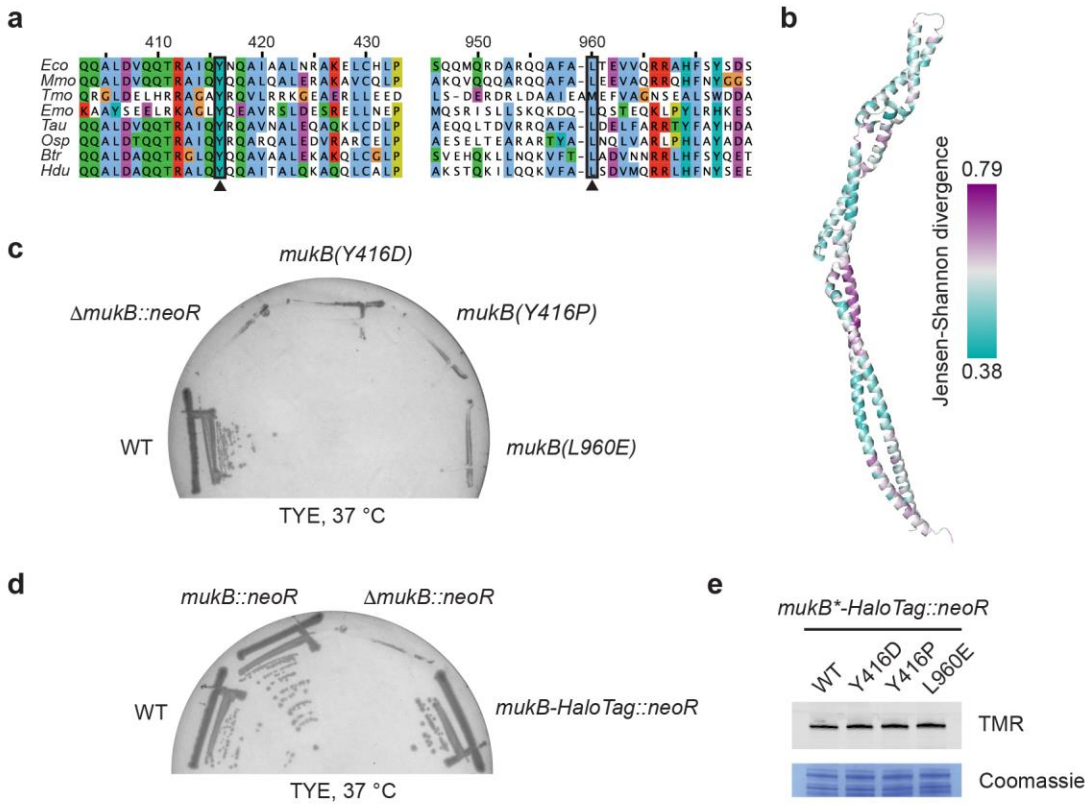

Supplementary Figure 3

Conservation analysis and mutagenesis of the MukB elbow.

a, Sequence alignment of the N-terminal (left) and C-terminal (right) parts of the MukB elbow. Residues chosen for mutagenesis are highlighted by triangles. *Eco*, *Escherichia coli*; *Mmo, Morganella morganii*; *Tmo*, *Thioflavicoccus mobilis*; *Emo*, *Endozoicomonas montiporae*; *Tau*, *Tolumonas auensis*; *Osp*, *Oceanimonas sp.* GK1; *Btr*, *Bibersteinia trehalosi*; *Hdu*, *Haemophilus ducreyi*. **b**, Sequence conservation (Jensen-Shannon divergence) was mapped onto the structure (high conservation is purple, low conservation is cyan). **c**, Growth of strains containing point mutations at the elbow in the endogenous *mukB* gene. **d**, Construction of a functional *mukB-HaloTag* allele. **e**, Protein levels of elbow mutants fused to a HaloTag. Extracts were labelled with a HaloTag-TMR substrate and were analyzed by in-gel fluorescence (top) and Coomassie staining (bottom) after SDS-PAGE. WT, wild-type.

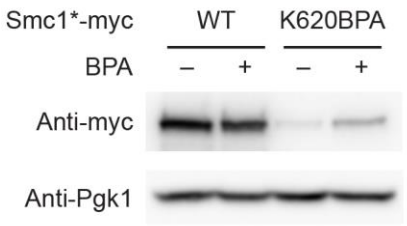

Supplementary Figure 4

BPA-dependent expression of Smc1(K620BPA).

Strains were grown either in the absence or presence of 1 mM BPA, and extracts were analyzed by Western blotting.

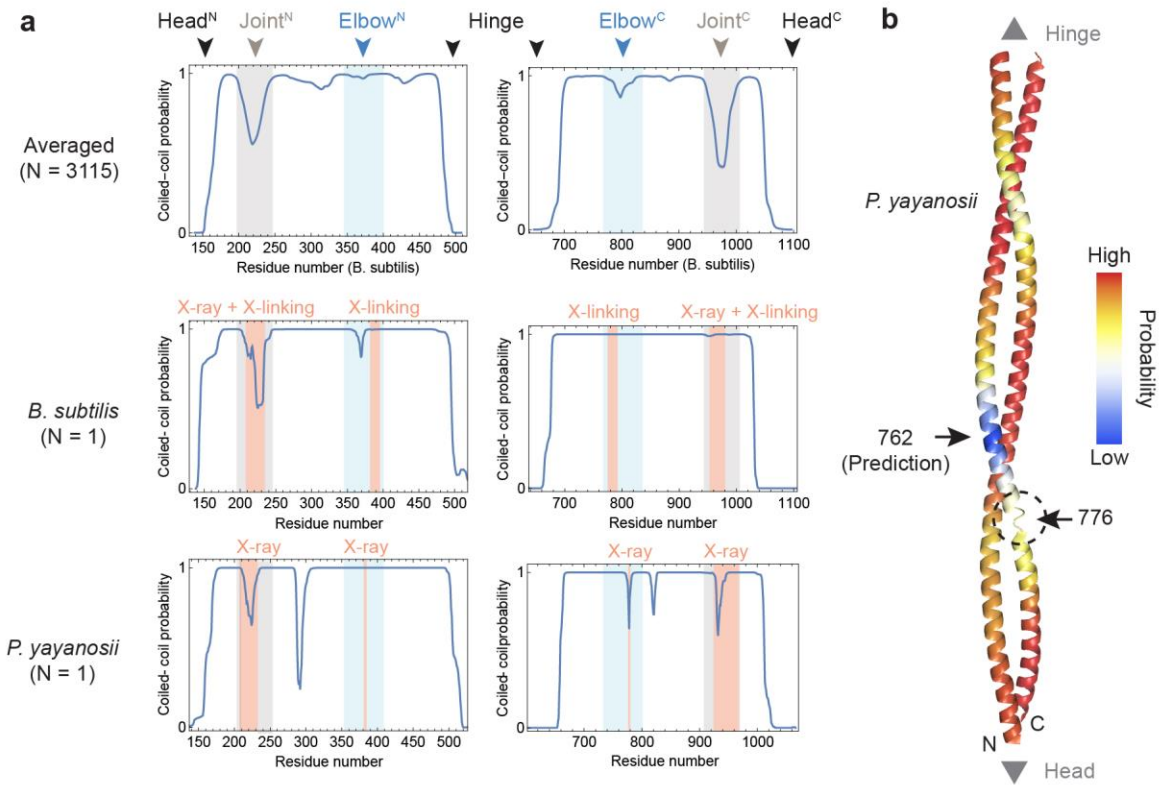

Supplementary Figure 5

Locations of coiled-coil discontinuities in bacterial and archaeal Smc proteins.

a, Aggregate coiled-coil probability profile (same as in Fig. 5) and single-sequence profiles for *B. subtilis* Smc (bacterial) and *Pyrococcus yayanosii* Smc (archaeal). Positions of coiled-coil discontinuities experimentally determined by X-ray crystallography (*Mol. Cell* **67**, 334-347.e5, 2017) or disulfide cross-linking (*Proteins* **83**, 1027–1045, 2015) are highlighted in red. **b**, The elbow region of *P. yayanosii* Smc. The predicted coiled-coil probability from aggregate analysis (see **a** and Fig. 5) is mapped onto the crystal structure of a central arm fragment (PDB ID 5XG2). Positions of the predicted and crystallographically determined discontinuities are shown.

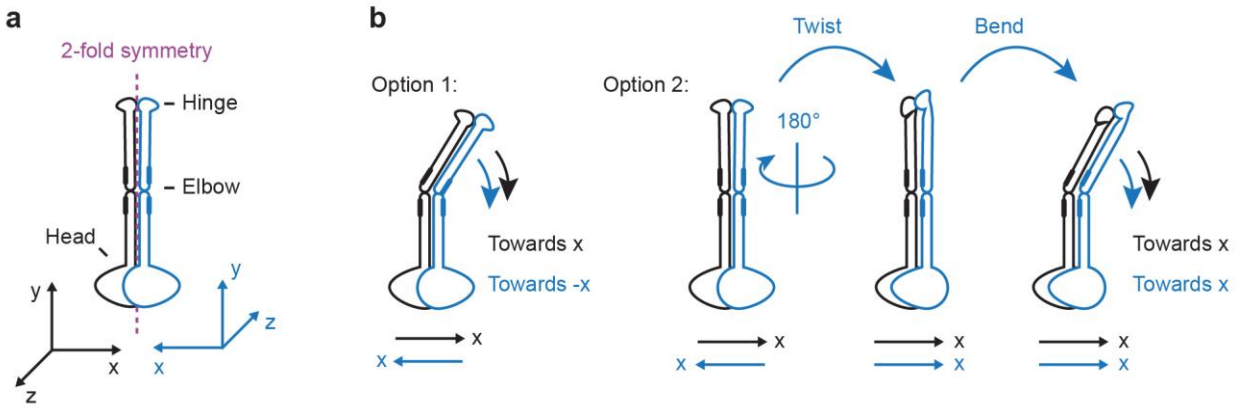

Supplementary Figure 6

Bending of SMC dimers.

a, An SMC dimer with C2 symmetry. Monomers and their body-frame coordinate systems are shown in black or blue. The symmetry axis of the dimer is shown in purple. **b**, Symmetry breaking upon elbow bending. Option 1: monomers bend into opposite directions; Option 2: monomers twist and bend into the same direction. Orientations of the relevant body-frame coordinate axes are shown at the bottom.

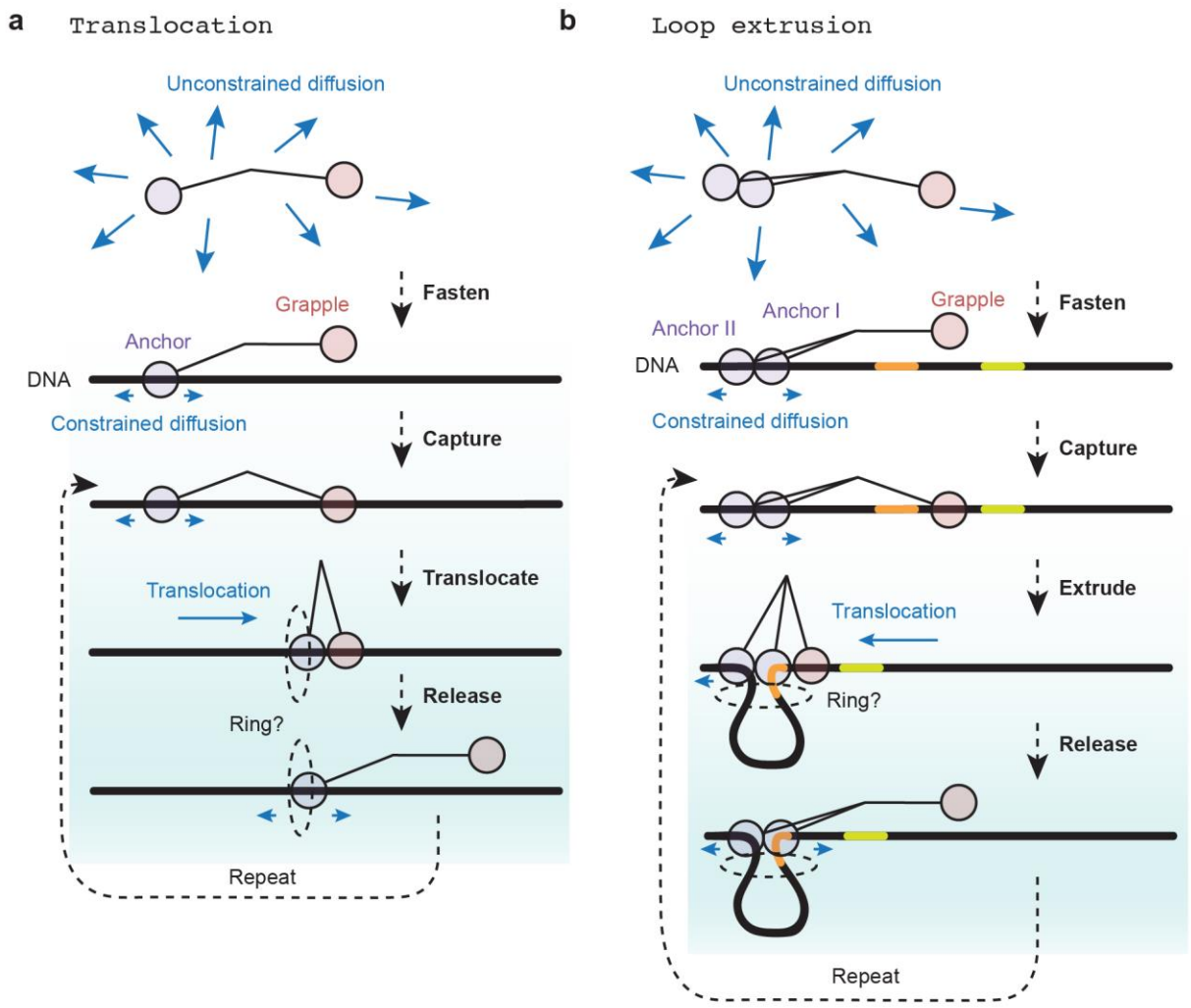

Supplementary Figure 7

Inchworm models for DNA and translocation and loop extrusion.

a, DNA translocation model requiring a regulated grapple DNA binding site and a sliding anchor DNA binding site. DNA binding may or may not involve a DNA entrapping ring that could be used to enhance processivity. **b**, Loop extrusion using a second anchor site. DNA binding may or may not involve a DNA entrapping ring that could be used to enhance processivity.

Fig. 1a

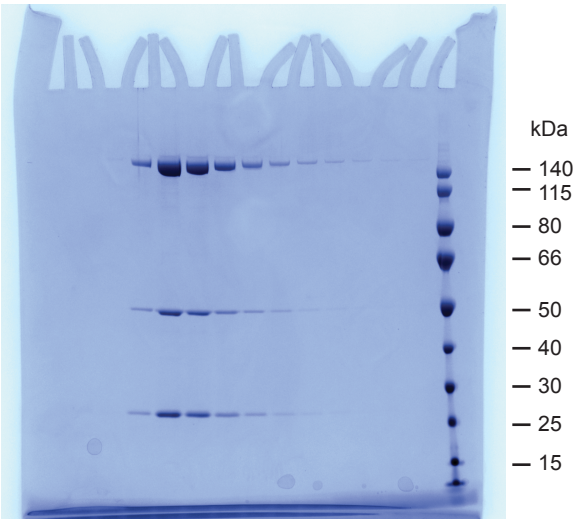

Fig. 4b

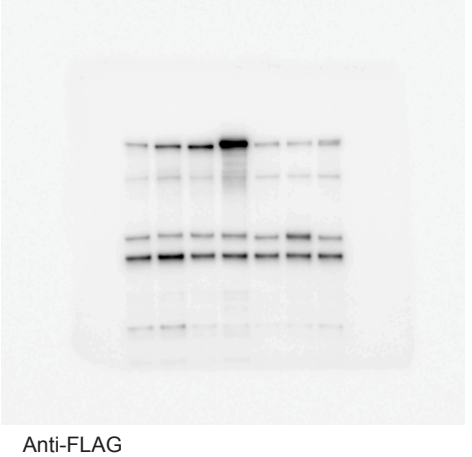

Anti-FLAG

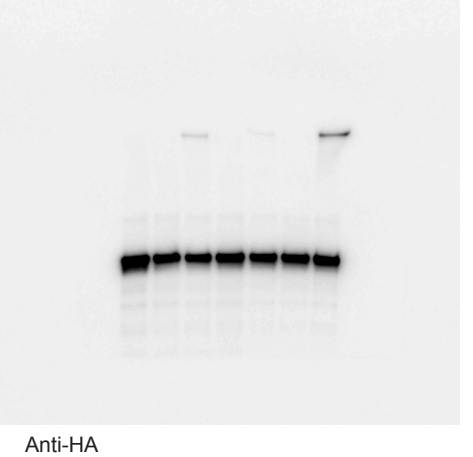

Anti-HA

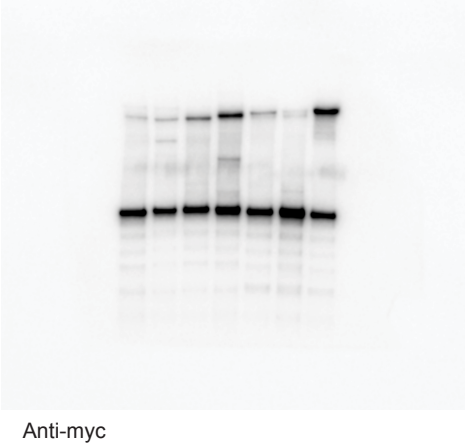

Anti-myc

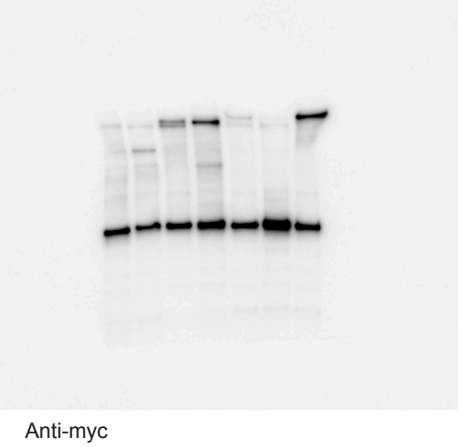

Anti-myc

Fig. 4c

Anti-FLAG

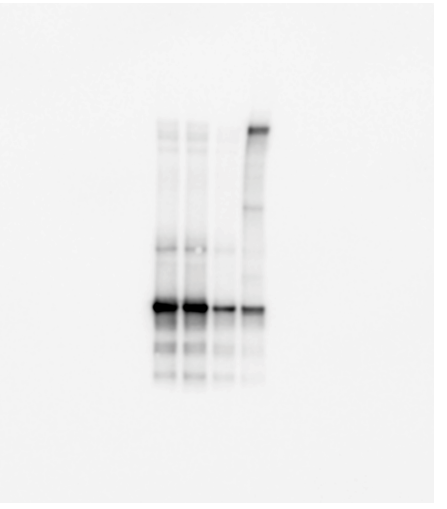

Anti-myc

Fig. 4d

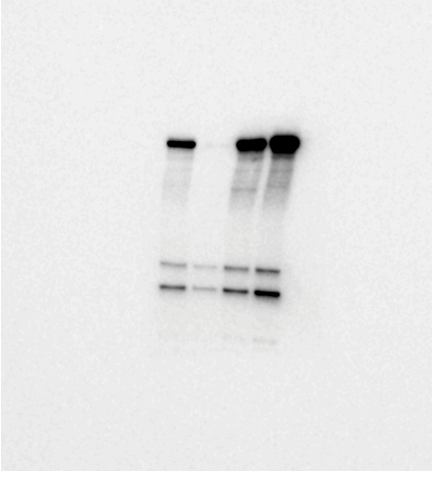

Anti-FLAG

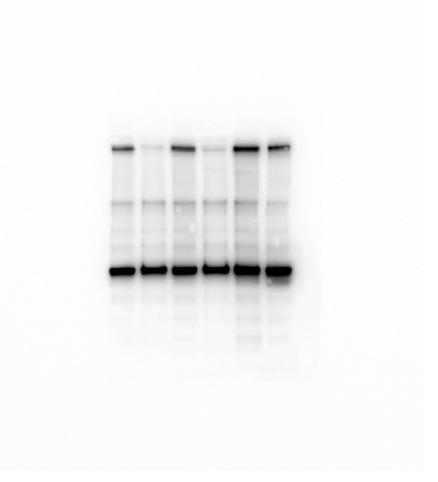

Anti-myc

Supplementary Table 1 | Microbial strains.

Strain ID	Genotype	Figures
***E. coli* strains**		
MG1655	F-, λ-, *rph*-1, *fnr+*	**S3c, S3d**
SFB012	MG1655, *mukB::neoR*	**S3d**
SFB017	MG1655, *mukB-HaloTag(C61V, C262A)::neoR*	**S3d, S3e**
SFB018	MG1655, *ΔmukB::neoR*	**S3c, S3d**
SFB022	MG1655, *mukB(Y416D)*	**S3c**
SFB025	MG1655, *mukB(Y416P)*	**S3c**
SFB026	MG1655, *mukB(L960E)*	**S3c**
SFB030	MG1655, *mukB(Y416D)-HaloTag(C61V, C262A)::neoR*	**S3e**
SFB031	MG1655, *mukB(Y416P)-HaloTag(C61V, C262A)::neoR*	**S3e**
SFB032	MG1655, *mukB(L960E)-HaloTag(C61V, C262A)::neoR*	**S3e**
***S. cerevisiae* strains**		
W303	*Mat a, ade2-1, trp1-1, can1-100, leu2-3, 112, his3-11, 15, ura3, GAL, psi*	**-**
2017	W303, Smc3-HA6::HIS3, Scc1-PK9::NatMX, pBH826 (Smc1(D588TAG)-myc9 in YEplac181), pBH61 (BPA cross-link, Trp1)	**4b**
2018	W303, Smc3-HA6::HIS3, Scc1-PK9::NatMX, pBH827 (Smc1(E562TAG)-myc9 in YEplac181), pBH61 (BPA cross-link, Trp1)	**4b**
2019	W303, Smc3-HA6::HIS3, Scc1-PK9::NatMX, pBH828 (Smc1(T565TAG)-myc9 in YEplac181), pBH61 (BPA cross-link, Trp1)	**4b**
2020	W303, Smc3-HA6::HIS3, Scc1-PK9::NatMX, pBH829 (Smc1(K620TAG)-myc9 in YEplac181), pBH61 (BPA cross-link, Trp1)	**4b**
2021	W303, Smc3-HA6::HIS3, Scc1-PK9::NatMX, pBH830 (Smc1(E591TAG)-myc9 in YEplac181), pBH61 (BPA cross-link, Trp1)	**4b**
2022	W303, Smc3-HA6::HIS3, Scc1-PK9::NatMX, pBH831 (Smc1(D592TAG)-myc9 in YEplac181), pBH61 (BPA cross-link, Trp1)	**4b**
2023	W303, Smc3-HA6::HIS3, Scc1-PK9::NatMX, pBH832 (Smc1(D593TAG)-myc9 in YEplac181), pBH61 (BPA cross-link, Trp1)	**4b**
2069	W303, Pds5-6xHis-6xFLAG::KanMX, Scc1-PK9::NatMX, pBH826 (Smc1(D588TAG)-myc9 in YEplac181), pBH61 (BPA cross-link, Trp1)	**4b**
2070	W303, Pds5-6xHis-6xFLAG::KanMX, Scc1-PK9::NatMX, pBH827 (Smc1(E562TAG)-myc9 in YEplac181), pBH61 (BPA crosslink, Trp1)	**4b**
2071	W303, Pds5-6xHis-6xFLAG::KanMX, Scc1-PK9::NatMX, pBH828 (Smc1(T565TAG)-myc9 in YEplac181), pBH61 (BPA cross-link, Trp1)	**4b**
2072	W303, Pds5-6xHis-6xFLAG::KanMX, Scc1-PK9::NatMX, pBH829 (Smc1(K620TAG)-myc9 in YEplac181), pBH61 (BPA cross-link, Trp1)	**4b, c, S4**
2073	W303, Pds5-6xHis-6xFLAG::KanMX, Scc1-PK9::NatMX, pBH830 (Smc1(E591TAG)-myc9 in YEplac181), pBH61 (BPA cross-link, Trp1)	**4b**
2074	W303, Pds5-6xHis-6xFLAG::KanMX, Scc1-PK9::NatMX, pBH831 (Smc1(D592TAG)-myc9 in YEplac181), pBH61 (BPA cross-link, Trp1)	**4b**
2075	W303, Pds5-6xHis-6xFLAG::KanMX, Scc1-PK9::NatMX, pBH832 (Smc1(D593TAG)-myc9 in YEplac181), pBH61 (BPA cross-link, Trp1)	**4b**
2221	W303, Pds5-6xHis-6xFLAG::KanMX, ura3::Scc1-PK9::URA3, pBH829 (Smc1(K620TAG)-myc9 in YEplac181), pBH61 (BPA cross-link, Trp1)	**4d**
2223	W303, Pds5-6xHis-6xFLAG::KanMX, ura3::Scc1(V137K)-PK9::URA3, pBH829 (Smc1(K620TAG)-myc9 in YEplac181), pBH61 (BPA cross-link, Trp1)	**4d**
2357	W303, Pds5-6xHis-6xFLAG::KanMX, Scc1-PK9::NatMX, pBH768 (Smc1-myc9 in YEplac181), pBH61 (BPA cross-link, Trp1)	**4c, S4**